MASTER'S THESIS

Near and intermediate field Evolution of a negatively buoyant jet

Laboratory experiment and mathematical modeling

Jacopo Grazioli and Davide Noro

Water Resources Engineering

Department of Building and Environmental Technology

Faculty of Engineering, Lund University

List of figures

List of tables

Abstract

The purpose of this study is to explore the behavior of a dense jet and bottom plume, composed of brine water, discharged into a receiving body of lighter fresh water. This situation is common in connection with freshwater production from sea water (desalination), which produces a brine waste stream, usually discharged into sea water.

The increasing interest in desalination processes requires investigations on how to reduce the negative impacts deriving from the brine discharge, appearing as a negatively buoyant jet. In this study a mathematical model was developed to simulate the jet and plume behavior in order to determine the optimum discharge conditions for different scenarios.

The model was divided into two sub-models, describing respectively the near and intermediate field properties of the discharge. Equations utilized are mass and momentum conservation, and several assumptions were made in order to simplify the mathematical description. The predictions of the model were compared with data collected at the Water Resources Engineering (TVRL) laboratory as well as results obtained with a commercial software simulation package (CORMIX®).

After the calibration of the main parameters, the model satisfactorily reproduced the experimental data, although the simulations are not able to adequately describe the effects of one important parameter, that is, the bottom slope. To overcome this problem separate calibrations are done with and without the bottom slope.

The main conclusions of this work are that the model produces results in acceptable agreement with data and observations, even though some improvements should be made in order to give the correct weight to the bottom slope parameter and to reduce the need for user calibration. An overall assessment of the CORMIX® software behavior cannot be made; in our case (*i.e.* small scale) the software was not giving simulation results that reproduced the data.

Acknowledgments

I want to thank Professor Magnus Larson and Professor Kenneth Persson at TVRL, who have been the supervisors for this thesis, and Raed Alshaaer, PHD student in the department and our leader for the experimental part. Thanks also to our office mates Marion, Andrej, and Ashenafi for all the company and moral support!

Also, I would like to thank Center for Middle East Study (CMES) at Lund University because the project was partly funded by them, primarily the experimental work.

And finally I want to thank our families, our friends, and girlfriends who were always close despite the distance.

1 Introduction

In recent years, usage of sea water as a source for water supply has constantly been increasing, thanks to the development of desalination processes. The desalination process brings as output fresh water from one side and brine water on the other side; the latter is effectively waste to dispose. The disposal of brines directly into the sea can increase the salinity level in the proximity of the output, alter the ecosystem equilibrium, and bring losses in efficiency of the desalination plant, if the sea water uptake is influenced by this change.

1.1 Background

At present in the world, about 3 billion people have only indirect access to fresh water and among these 1.76 billion live in areas affected by serious water scarcity (Charcosset, 2009). Water scarcity is effective when people cannot satisfy their need of water for drinking, washing, and general life activities, and where this lack lasts for consistent periods of time (Rijsberman, 2006). This phenomenon is understandable considering that in nature only 1 % of the world-wide water is usable by humans, and 99 % of that is underground water, not always easily accessible.
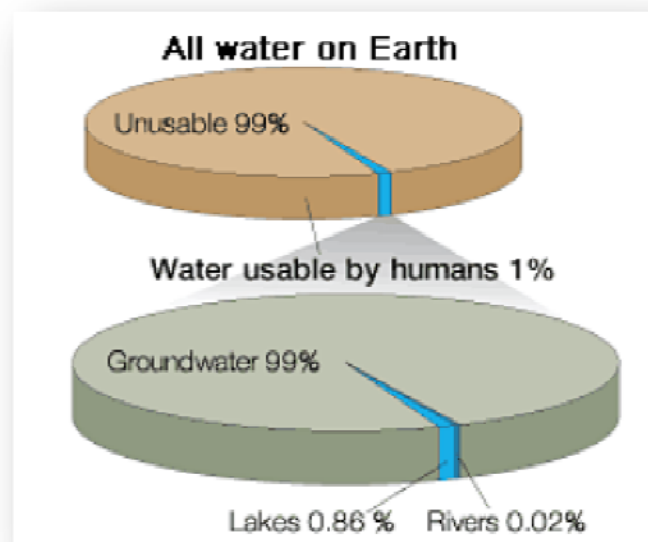
Figure 1 Water distribution in the world (ref U.S. department of the interior)

When the commonly used sources of fresh water (*e.g.*, lakes, rivers, and underground aquifers) are not available, desalination of sea water can be a significant source for water supply.

By definition: "Desalination is the process of removing dissolved salt and other minerals from seawater to create freshwater." (water-technology.net). Desalination found large-scale application for the first time in the 1920´s and 1930´s, and it grew fast as technological development and population needs did.

Nowadays the world cumulative contracted capacity of desalination plants is more than 60 millions of m^3 per day, referring to sea water (IDA‟s Desalination Yearbook, 2008-2009). Almost 90 % of existent plants are situated in a relatively small area, which is Europe (10 %), North Africa, and the Middle East (77 %) (Lattermann, 2007).

The spreading of this technology is illustrated in figure 2, which shows the effective production from existing plants and its evolution in the last years. Contracted capacity can differ from the effective one and gives us information only about the fresh water flux, *i.e..*, the output.
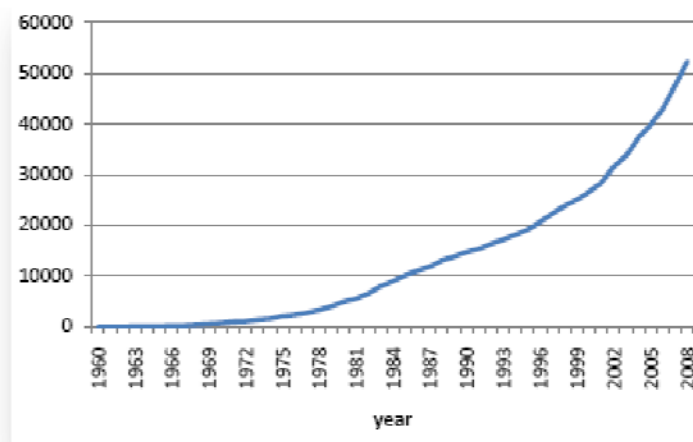
Figure 2 Production of desalinated water in million m^3 through time (ref IDA s desalination yearly book 2008-2009)

1.1.1 Desalination technology

In a desalination plant seawater is taken and separated in two different outputs: a fresh water stream with low concentration of dissolved salts and, as a waste stream, brine water with high concentration of salts. This separation is energy consuming and different technologies have been

developed to perform the separation, but in the future only three processes will be dominant (Khawaji *et al,* 2008):

> ➤ Multi stage flash distillation (MSF)
> ➤ Reverse osmosis (RO)
> ➤ Multiple effect distillation (MED)

It is important to have an approximate overall estimate of the different streams, and according to 2009 data presented by Bashitialshaaer *et al.* (2009):

Let Q_I; Q_F; Q_B be, respectively, input, fresh, and brine streams in 1000 m^3 / day, then the world wide values are Q_I = 120000; Q_F = 48000; Q_B = 72000. Defining the recovery ratio as r = Q_F / Q_I and assuming that fresh water will have a salinity of S_F < 300 mg / l (*i.e.*., negligible with respect to the mean sea water value of about 35000 ppm), the salinity of the brine stream will be S_B = S_I / (1-r); (as an example using the data presented above, r = 0.4 and S_B = 58000 ppm).

1.1.2 Desalination in Italy

Desalination activities in Italy are mainly located to the southern part and in the islands. Systematic research on desalination first began in 1965, and water supply started to be studied in-depth by the "Water Research Institute" (Di Pinto, 1977). Up to now in Italy, there are about 70 desalination plants active, yielding a total production of 420 t/d in terms of fresh water. There is not, however, a well organized and centralized plan of investment in this field, but every year there are built, in average, 2 or 3 additional plants (Rognoni, 2009). It follows that in the next years desalination will play a larger role in the overall water supply.

1.2 Objective

The present thesis focuses on the discharge of the residue brine water and on the modeling of its evolution in space downstream the discharge area.

The overall objective of this work is the investigation of the behavior of a negatively buoyant jet, and the following bottom plume ideally composed of brine water from a desalination plant. The investigation will focus on the lateral spreading (perpendicular to jet or plume axis) and the evolution of the salinity concentration on the centerline. This kind of analysis will help to find the most effective parameters influencing spreading and mixing, in order to design a proper discharge system.

The detailed objectives can be summarized as:

➢ Develop a mathematical model to describe lateral spreading and centerline dilution of buoyant jet and plumes for near and intermediate field

➢ Run a set of laboratory experiments, simulating discharge conditions in bench scale

➢ Find out possible correlation of measured values with non-dimensional numbers, *e.g.* densimetric Froude and Reynolds numbers

➢ Observe the effect of main parameter variation on spreading and dilution properties

➢ Calibrate the mathematical model with data collected in the laboratory, and test it on a different set of data

➢ Compare measured data and modeled data with simulation results obtained using the software CORMIX[®]

1.3 Procedure

A literature survey was made regarding near-field and intermediate field properties of negatively buoyant jets and bottom plumes focusing on brine discharge from desalination plants. Data on jet and plume evolution, including dilution and mixing were compiled.

A set of experiments was performed at the Water Resources Engineering (TVRL) laboratory at a reduced scale. A mathematical model of the jet spreading and dilution was developed. It is based on the mass and momentum conservation equations, and it is divided into two sub-models describing the near and intermediate field. The model was subjected to sensitivity analysis, then calibrated and validated towards the literature data base, to some extent, and the additional data collected in the present experiments. It is investigated whether or not errors between calculated and simulated data are related to any specific geometrical parameter or non-dimensional number.

Also, a general survey on the possible correlation between measured values and various non-dimensional numbers, for example, the densimetric Froude or Reynolds numbers is made.

Furthermore, data from the model and the experiments are compared with simulation results obtained with the software CORMIX[®], and the application to small-scale experiments is discussed.

2   Discharge of brine from desalination plants

2.1   Generalities

When the discharge takes place in sufficiently large receiving water it is possible to distinguish between three different zones for the discharge. In the first zone, called the near field, the release is controlled by the jet properties: the buoyancy caused by the density difference, the momentum flux, and the geometry of the diffuser. These parameters are able to control the jet diffusion and the primary dilution that is the most important to guarantee a good mixing of the brine with the brackish waters. The 3rd zone (far field) is characterized by greater time and length scales compared to the near-field and this zone can extend many kilometers from the discharge point. In this area the initial conditions of the jet are no more important and the dilution is driven by the magnitude of the ambient currents. As a result, normally the rate of dilution is much lower compared to the near field; however, it could be highly variable in the presence of particularly strong currents. The 2nd zone, called intermediate field, is a transition region between the near field and the far field, and it will be discussed further later on in the report.

To define the location where one zone ends and another one starts is not easy, and it depends on how the brine is discharged in the receiving water (*e.g.* parallel to the bottom or released at a discharge angle with respect to the bed of the sea) and on the general characteristic of the receiving water body itself.

2.2   Impacts

The greatest environmental concerns related to the discharge from a desalination plant are the very high concentration of salts that are found in the brine as a result of the desalination process. Thus, it becomes important to reduce the impact closest to the discharge point to avoid the creation of a stratified system that can affect the benthic communities unused to changes in salinity. Recently, there has been a lot of discussion in the literature on this issue, and Torquemada *et al.* (2005) and Latorre (2005) have carefully investigated how the higher concentration of salt could affect the vitality of some of the most sensitive biological organisms

in the Mediterranean Sea. The results they obtained showed that species vitality was influenced within the first year of monitoring.

A potential reduction of the brine impact on the marine environment could be achieved with the collection and transportation of the brine to a saltworks as stated by Laspidou *et al.* (2010). In this case it is important to define if it is a feasible solution considering that for human consumption appropriate treatments should be taken in account.

Another environmental aspect to take into consideration with regard to brine discharge is the chemicals used in the various phases, *i.e.* anti-scaling, antifouling, hydrochloric acid, and sodium hexametaphosphate. These chemical products are used mainly to avoid scaling on the pipes and on the membrane in Reverse Osmosis plants or to remove all the suspended biological matter that could grow, creating problems for the treatment.

3 Near-field and intermediate field properties of negatively buoyant jets

3.1 Previous studies

Previous studies mainly focussed on the separate analysis of near-field and intermediate-field properties of buoyant jets and plumes. Some hypotheses on how to connect the two different zones have also been proposed. Many studies investigated the main properties of submerged jets using non-dimensional numbers and developed empirical relationships based on such numbers.

3.1.1 Mathematical modeling

Cipollina *et al.* (2004) presented a model based on the conservation of mass, volume flux, momentum and buoyancy flux, describing the evolution of a buoyant jet in the near field of the discharge, validating the model against laboratory data. Sanchez (2009) developed a similar model, and for the model testing data collected in the laboratory were employed, as well as data from Cipollina *et al.* (2004). He employed a range of entrainment coefficients in the model testing obtained from previous studies.

Christodoulou (1991) described theoretically the main factors affecting near-, intermediate-, and far-field properties, suggesting appropriate length scales for each zone. A procedure for matching between the near and intermediate field was also proposed, together with an equation (used in the present thesis work) describing the conservation of the momentum flux in the intermediate field, also discussing the lateral spreading of the plume.

Baines (1985) studied the entrainment of ambient water into buoyant jets through laboratory experiments, describing the effects on this parameter from the geometry of the system and the presence of boundaries.

Purnama and Barwani (2004) investigated a model based on diffusion, *i.e.* not describing the shape of the jet, but focusing on the dilution at different distances from the discharge point. The effects of a constant tidal current were investigated and included in the model, and solutions were proposed in order to increase the dilution.

Bleninger and Jirka (2007) developed a software called CORMIX® to calculate jet trajectories and dilutions rates for general purpose applications in engineering projects.

3.1.2 Dimensional analysis

Cipollina *et al.* (2005) studied the relationship between some characteristic geometric parameters describing a buoyant jet trajectory in the near field (*i.e.* impact point or point of maximum elevation) and the densimetric Froude number of the discharge. They found a strong linear correlation between these quantities and the densimetric Froude number. The effects of the jet viscosity on the trajectory behavior were also discussed.

Sanchez (2009) employed a similar type of analysis, focusing on the effects on the geometric parameters with regard to the densimetric Froude number. Furthermore, the relation between these parameters and the Reynolds numbers were shown to be weak.

Suresh *et al.* (2008) investigated the lateral spreading of plane buoyant jets and how they depend on the Reynolds number, suggesting and demonstrating that a reduction of the spreading occurs with an increase in the Reynolds number.

3.2 Near-field

Jet behavior in the near field has been the object of many studies in the last years, depending primarily on the fact that the jet properties are being governed by the discharge arrangements, such as the depth of discharge, the type and number of diffusers, and the initial flux of volume, momentum, and buoyancy. Thus, there is some possibility to control the dilution in the near field. The dilution and mixing of brines in the near field are due to entrainment of ambient water into the jet.

In the literature the near-field has been thoroughly investigated since it is an important zone for obtaining significant mixing of the brine with the receiving water. Sanchez (2009), for example, studied the effects of the initial jet angle on the trajectory in a laboratory experiment, which has large implications for the mixing and dilution rate achieved, providing insights to the selection of an optimal discharge configuration.

In this study, the main importance of investigating the near field was to determine where the flux was becoming mostly influenced by the buoyant forces and where the buoyant jet witched into a bottom plume. The experimental data were compared to classical jet theory with the help of the CORMIX® software to validate the governing mathematical equations and to understand the

processes involved. Figure 3 illustrates the transition between a buoyant jet in the near field and the unsteady spreading characteristic in the intermediate and far field. However, for brine disposal the buoyancy is negative, inducing a bottom plume when the jet hits the bed.
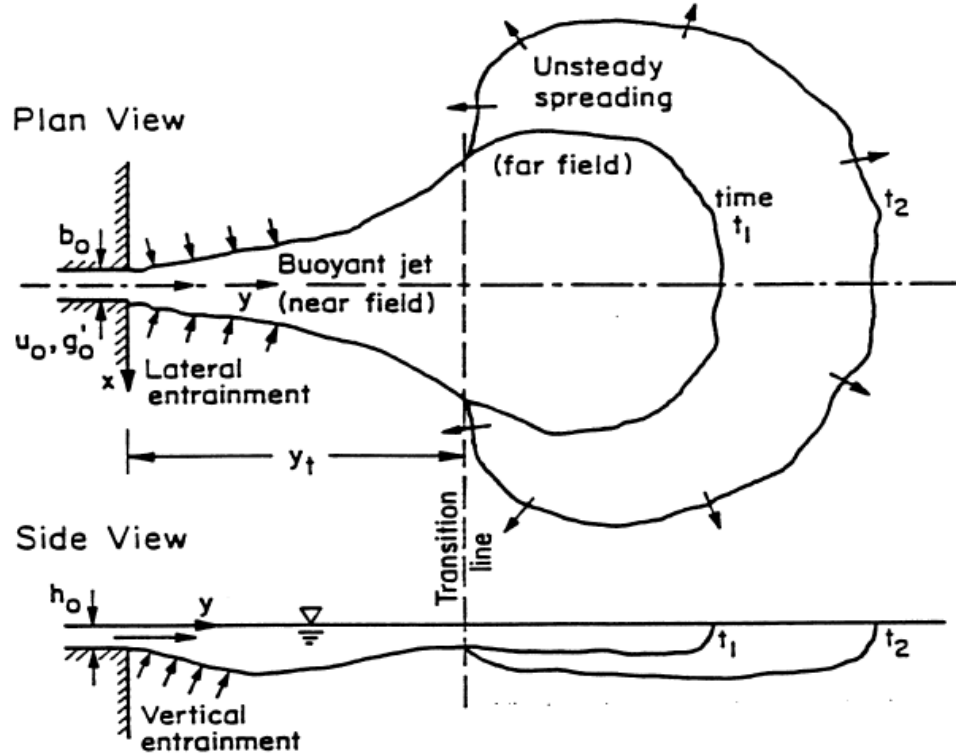
Figure 3 Near and far field evolution for a buoyant discharge (Doneker and Jirka, 2007)

3.3 Intermediate field

The intermediate field is where the initial near-field jet flux properties are slowly changing into a bottom density plume subject to passive diffusion, the main process governing jet evolution at a certain distance from the source point. This mixing zone extension is difficult to define as it is greatly dependent upon the initial conditions of the jet and the ambient influences. Christoudoulou (1991) suggested as starting point for the intermediate field the point of interaction between the negatively buoyant jet and bottom, and stated that the total length of the field is inversely proportional to the drag coefficient C_D. In our laboratory experiment (described in chapter 5) the absence of any ambient forcing, for example, wind or current, together with a glass bottom with a low drag coefficient, prevented the far field to completely develop. As a

result the transitional (intermediate) zone is assumed to have extended the entire length of the tank.

3.4 Far field

Even if the far field is not of direct interest in this study, is useful to give a small description for the sake of completeness.

As previously stated, not many studies have been conducted in the far field concerning brine disposal due to the nature of the transport and mixing processes, which are mainly dominated by advection from ambient currents and mixing from ambient diffusion processes.

Ambient currents could be generated by wind, waves, and tides. However, the advection may also result as "spreading processes arise due to the buoyant forces caused by the density difference of the mixed flow relative to the ambient density" (Doneker and Jirka, 2007).

The mixing occurs quite slowly compared with the ambient water entrainment in the near-field
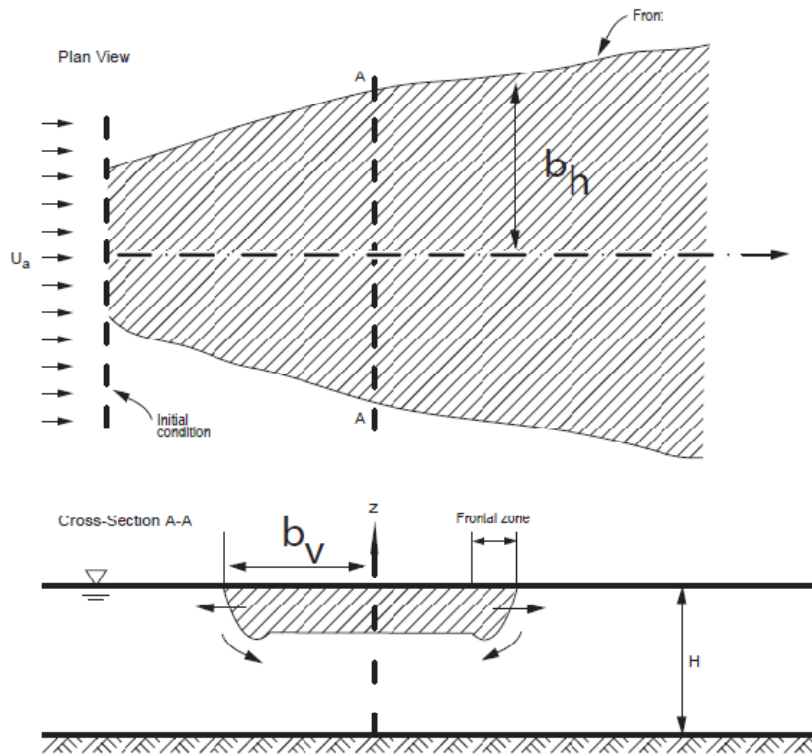
Figure 4 Buoyant spreading processes downstream of the intermediate-field region (Doneker and Jirka, 2007)

17

zone and it is also limited to the "head" of the flow, as shown in figure 4. If an ambient stratification is not present, the only process affecting the dilution is the passive diffusion.

Passive ambient diffusion becomes the dominant process after a sufficient distance from the release point and it produces an increase in thickness and width until the discharged flow interacts with the shore or the bottom. The flow development can be described by the 4/3 law of diffusion for which the diffusivity is plume-size dependent. However, for narrow estuaries the flow is better described through a constant diffusivity in the vertical and horizontal direction, as observed by Doneker and Jirka (2007).

4 Mathematical modeling of lateral spreading and dilution in near and intermediate field

Mathematical modeling of the jet and plume evolution was essentially divided into two sub-models. In the near field, in the proximity of the nozzle, jet and plume development is driven by the initial conditions; *i.e.* the initial momentum flux, volume flux, and buoyancy flux, and there is no interaction with the bottom. In the intermediate field the buoyant jet essentially becomes a plume and it is interacting with the bottom and the main forces to be taken into account are bottom drag force and bottom slope effects.

4.1 Near-field modeling of buoyant jet evolution

4.1.1 Model assumption

In order to develop a simple model describing the situation in the proximity of the discharge nozzle, some assumptions are made following to Jönsson (2004):

- ➢ Hydrostatic pressure distribution in the ambient water and in the jet.
- ➢ Small variation of density inside the jet, compared to the receiving water density.
- ➢ Density differences are too small to affect inertia forces, but are important for the buoyancy force (the Boussinesque approximation). This assumption implies that the continuity equation can be described in terms of volume instead of mass
- ➢ Horizontal momentum of the jet is constant along the jet trajectory.
- ➢ Jet is symmetrical in a plane perpendicular to the jet axis.
- ➢ There is similarity for velocities and concentrations (or density deficit) in planes perpendicular to the jet axis (Gaussians distributions).
- ➢ There is no influence from the boundaries of the receiving water.
- ➢ There is a linear relationship between concentration and density.

4.1.2 Mathematical basics

The jet velocity and salt concentration in this sub-model are following Gaussian distributions:

$$u = u_m \cdot e^{-\left(\frac{r}{r_u}\right)^2} \tag{1}$$

$$C = C_m \cdot e^{-\left(\frac{r}{r_c}\right)^2} \qquad (2)$$

Where:

r is the transverse or radial distance from the jet axis

u is the velocity at r u_m is the maximum velocity in the jet (this velocity occurs at the jet centerline)

r_u is the characteristic jet width for velocity

c is the concentration at r

C_m is the maximum concentration which can be found at the jet centerline

r_c is the characteristic jet width for concentration

Also, the typical value for a jet is:

$$\lambda = \left(\frac{r_c}{r_u}\right) = 1.2 \qquad (3)$$

The assumed linear relationship between density and concentration is expressed as:

$$\rho = \rho_a + k \cdot C \qquad (4)$$

Where:

ρ is the jet density

ρ_a is the ambient water density

k is a constant, experimentally obtained in our case to be 0.537, if the concentration is expressed in Electrical Conductivity (EC). The linear relationship can be accepted in the range under consideration.

C is the salt concentration, in this case indirectly described by the EC

4.1.3 Mass conservation for water and tracer

The following equations describe the conservation of water volume, *i.e.* the continuity equation (see hypothesis) and tracer mass flux.
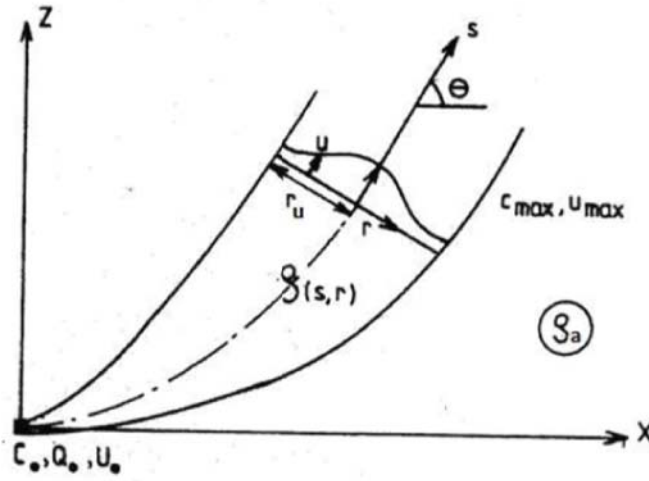
Figure 5 Definition sketch for a circular buoyant jet (Jonsson, 2004)

The continuity equation for water describes how the volume water flux is increasing by the entrainment of ambient water, which is taken proportional to velocity at contact lateral interface. Water is considered to be incompressible.

$$\frac{dQ}{ds} = \alpha \cdot u_m \cdot 2\pi \cdot r_u \tag{5}$$

Where:

Q is the flow in the jet

s is the coordinate following the jet axis, *i.e.* along the trajectory

α is the entrainment coefficient

Equation (5) is developed in this way, omitting all steps:

$$Q = \int_0^\infty u_m \cdot e^{-\left(\frac{r}{r_u}\right)^2} \cdot 2\pi \cdot r \, . \, dr = \pi \cdot u_m \cdot r_u^2 \tag{6}$$

Substituting (6) into (5) yields:

$$\frac{d}{ds}(u_m \cdot r_u^2) = 2\alpha \cdot u_m \cdot r_u \tag{7}$$

The mass conservation equation for the tracer is expressed as:

$$\frac{d}{ds} \int_0^\infty C_m \cdot e^{-\left(\frac{r}{r_c}\right)^2} \cdot u_m \cdot e^{-\left(\frac{r}{r_u}\right)^2} 2\pi \cdot r \cdot dr = \frac{d}{ds} (\pi \cdot C_m \cdot u_m \cdot \frac{\lambda^2}{1+\lambda^2} \cdot r_u^2) = 0 \tag{8}$$

Considering that the quantity of tracer is constant in the jet and equal to the initial quantity discharged into ambient m_0:

$$m_0 = Q_0 \cdot C_0 \tag{9}$$

Equation (8) is reduced to:

$$\pi \cdot C_m \cdot u_m \cdot \frac{\lambda^2}{1+\lambda^2} \cdot r_u^2 = m_0 \tag{10}$$

4.1.4 Momentum conservation

The momentum equation in the x-direction is written:

$$\frac{d}{ds} \int_0^\infty (u^2 \cdot \rho \cdot 2\pi \cdot r \cdot \cos(\theta)) \cdot dr =$$

$$= \frac{d}{ds} \left[\rho \cdot 2\pi \cdot \int_0^\infty u_m^2 \cdot e^{-2\left(\frac{r}{r_u}\right)^2} \cdot r \cdot \cos(\theta) \, dr \right] =$$

$$= \frac{d}{ds} \left(\frac{\pi}{2} \cdot \rho \cdot u_m^2 \cdot r_u^2 \cdot \cos(\theta) \right) = 0 \tag{11}$$

This equation is easily solved imposing the equality with the initial momentum in the x-direction M_{0x}:

$$\frac{\pi}{2} \cdot \rho \cdot u_m^2 \cdot r_u^2 \cdot \cos(\theta) = M_{0x} \tag{12}$$

Where:

$$M_{0x} = \rho_0 \cdot \frac{Q_0^2}{A_0} \cdot \cos(\theta_0) \tag{13}$$

In which A_0 is the nozzle area, neglecting any contraction of jet at the discharge point.

The momentum equation in z-direction (vertical direction) is given by:

$$\frac{d}{ds} \int_0^\infty (u^2 \cdot \rho \cdot 2\pi \cdot r \cdot \sin(\theta)) \cdot dr = F_B' \tag{14}$$

The left part of the previous equation can be written, in analogy with the x-direction, as:

$$\frac{d}{ds}\left(\frac{\pi}{2} \cdot \rho \cdot u_m{}^2 \cdot r_u{}^2 \cdot \sin(\theta)\right) \tag{14b}$$

F_B' is the vertical buoyancy force acting on the jet. It depends on ambient water density, jet density, and gravity:

$$F_B' = \int_0^\infty g \cdot (\rho_a - \rho) \cdot 2\pi \cdot r \cdot dr \tag{15}$$

Using the linear relationship between density and concentration (4) and substituting in (15):

$$F_B' = -\int_0^\infty k \cdot C_m \cdot e^{-\left(\frac{r}{r_c}\right)^2} \cdot 2\pi \cdot r \cdot dr = -\pi \cdot g \cdot k \cdot C_{,m} \cdot r_c^2 \tag{16}$$

Finally combining equation (16) and (14b) we obtain:

$$\frac{d}{ds}\left(\frac{\pi}{2} \cdot \rho \cdot u_m{}^2 \cdot r_u{}^2 \cdot \sin(\theta)\right) = -\pi \cdot g \cdot k \cdot C_{,m} \cdot r_c^2$$

Assuming in this case that $\rho_a \cong \rho$

$$\frac{d}{ds}\left(u_m{}^2 \cdot r_u{}^2 \cdot \sin(\theta)\right) = -2 \cdot g \cdot \frac{k}{\rho_a} \cdot C_{,m} \cdot r_u^2 \cdot \lambda^2 \tag{17}$$

4.1.5 Governing equations

Governing equations (7), (10), (12), (17) for this part of the model are summarized below:

$$
\begin{cases}
\dfrac{d}{ds}(u_m \cdot r_u^2) = 2\alpha \cdot u_m \cdot r_u \\[2mm]
\pi \cdot C_m \cdot u_m \cdot \dfrac{\lambda^2}{1 + \lambda^2} \cdot r_u{}^2 = m_0 \\[2mm]
\dfrac{d}{ds}\left(u_m{}^2 \cdot r_u{}^2 \cdot \sin(\theta)\right) = -2 \cdot g \cdot \dfrac{k}{\rho_a} \cdot C_{,m} \cdot r_u^2 \cdot \lambda^2 \\[2mm]
\dfrac{\pi}{2} \cdot \rho \cdot u_m{}^2 \cdot r_u{}^2 \cdot \cos(\theta) = M_{0x}
\end{cases}
$$

Two equations describing the geometry of the jet must be added:

$$
\begin{cases}
\sin(\theta) = \dfrac{dz}{ds} \\[2mm]
\cos(\theta) = \dfrac{dx}{ds}
\end{cases}
$$

4.1.6 Solution of the governing equations

The system of equation to solve in this first part of the model is a set of ordinary differential equations, which can be solved using finite differences methods. Once solved, the system implemented is presented below, for the four unknowns Θ; C_m; u_m; r_u.

$$\theta_{i+1} = \arctan\left(\tan(\theta_i) - \frac{g \cdot k \cdot \lambda^2 \cdot \pi \cdot \rho_i}{\rho_a \cdot M_{0\,x}} \cdot \Delta s \cdot C_{m_i} \cdot r_{u_i}^2\right) \tag{18}$$

$$C_{m_{i+1}} = \frac{1}{\frac{1}{C_{m_i}} + \frac{2 \cdot \alpha \cdot \pi \cdot \lambda^2}{m_0 \cdot (1 + \lambda^2)} \cdot \Delta s \cdot u_{m_i} \cdot r_{u_i}} \tag{19}$$

$$u_{m_i} = \frac{2 \cdot M_{0\,x} \cdot \lambda^2 \cdot C_{m_i}}{\rho \cdot m_0 \cdot (1 + \lambda^2) \cdot \cos(\theta_{i+1})} \tag{20}$$

$$r_{u_i} = \frac{m_0 \cdot (1 + \lambda^2)}{\lambda^2 \cdot C_{m_i}} \cdot \sqrt{\frac{\rho_i \cdot \cos(\theta_{i+1})}{2 \cdot \pi \cdot M_{0\,x}}} \tag{21}$$

$$x_{i+1} = x_i + \Delta s \cdot \cos(\theta_i) \tag{22}$$

$$z_{i+1} = z_i + \Delta s \cdot \sin(\theta_i) \tag{23}$$

Where i is the number of a specific iteration (step along the jet trajectory). In this way the solution is calculated stepwise, starting from the nozzle outlet, where all the values are known. In our case, when attention is focused on lateral spreading and dilution, the unknowns of interest are r_u, which is representing the diameter of the jet and C_m. Last iteration is the one in which the jet reaches the bottom.

4.2 Intermediate field modeling of plume evolution

When the buoyant jet reaches the bottom and impinges upon it, the jet enters the region denoted as the intermediate field. Thus, intermediate field extends beyond the near field and eventually translates into the far field, at the point where lateral spreading ceases (Christodoulou, 1991).

Modeling of this second region (intermediate field), requires different assumptions and the setting of new initial conditions, obtained by matching the intermediate-field model with all the information carried from the last iteration by the near-field model.

4.2.1 Model assumptions

The main assumptions made in this sub-model are the following:

➢ Hydrostatic pressure distribution in the ambient water and in the jet (bottom plume).

➢ Small variation of density inside the plume, compared to the receiving water density.

➢ Continuity equation can be written in terms of volume.

➢ Plume is symmetrical in a plane perpendicular to the jet axis.

➢ The section of the plume is not anymore round-shaped but rectangular

➢ Plume is moving attached to the bottom; drag effect is taken into account by C_d.

➢ There is a linear relationship between concentration and density.

➢ Slope of the bottom is constant.

➢ Increase in volume flux is still described through entrainment of ambient water.

4.2.2   Matching between near field and intermediate field

A difficult point in using two different models to describe different phases of the same experiment is the necessity of obtaining continuity between the information carried at the end of the first model and the beginning of the second model.

In the second model, the cross section of the plume is considered to be rectangular, in spite of the round-shaped section used in the first (jet) model. The plume section has the following characteristics:

b is the half width of the plume (measured in y-direction, perpendicular to the flow axis)

h is the height or thickness of the plume (measured perpendicular to the bottom slope)

C is the average concentration of salt or of EC in the section

u is the average velocity in the section

Considering that this work is focused on modeling the lateral spreading and the dilution; in the matching between the two models, priority will be given to ensure continuity of C and b more than other quantities. According with this principle:

$$b_0 = r_{u_{last}}$$

$$u_0 = \frac{Q_{last}}{A_{last}} = \frac{1}{\pi \cdot r_{u_{last}}^2} \cdot \int_0^{r_{u_{last}}} u_m \cdot e^{-\left(\frac{r}{r_u}\right)^2} \cdot 2\pi \cdot r \ dr = u_{m \ last} \cdot (1 - e^{-1})$$

$$h_0 = \frac{Q_{last}}{u_0 \cdot 2 \cdot b_0} = \frac{\pi \cdot b_0}{2}$$

$$C_0 \cong C_{m \ last}$$

Where:

u_o, h_0, b_0, C_0 are the initial conditions for the intermediate field model

last- refers to the value of a quantity in the last iteration of the near field model
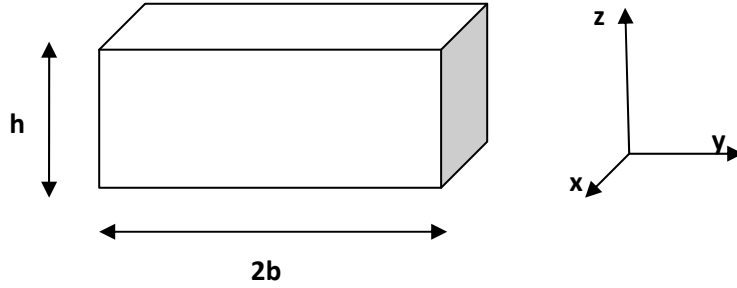
Figure 6 Sketch of intermediate field plume geometry

4.2.3 Mass conservation for water and tracer

Continuity equation for water will be adjusted to the new geometry and to the new conditions, and the entrainment coefficient will be a "plume" coefficient α_{plumes}, whereas in the first model it was α_{jet} , according to Taylor theory. Continuity is expressed as :

$$\frac{dQ}{ds} = \alpha_{plumes} \cdot u \cdot (2h + 2b) \tag{24}$$

This equation can be developed into:

$$\frac{d(u \cdot 2b \cdot h)}{ds} = \alpha_{plumes} \cdot u \cdot (2h + 2b) \tag{25}$$

Mass conservation for the tracer, considering that there is no reaction occurring and that the total mass of salt is constant in the jet, becomes:

$$m_0 = u \cdot 2b \cdot h \cdot C \tag{26}$$

4.2.4 Momentum conservation

Momentum conservation, assuming that the plume trajectory is parallel to the bottom, will take the form of (Christodoulou, 1991):

$$\frac{d(u^2 \cdot b \cdot h)}{ds} = \lambda^* \cdot \frac{\rho - \rho_a}{\rho_a} \cdot g \cdot 2b \cdot h \cdot \sin(\omega) - C_D \cdot u^2 \cdot 2b \tag{27}$$

26

Where:

λ^* is a density distribution factor of order 1

ω is the bottom slope

C_D is the coefficient of drag

4.2.5 Governing equations

The system of governing equations (27), (26), and (25) is summarized as:

$$\begin{cases} \dfrac{d(u^2 \cdot b \cdot h)}{ds} = \lambda^* \cdot \dfrac{\rho - \rho_a}{\rho_a} \cdot g \cdot 2b \cdot h \cdot \sin(\omega) - C_D \cdot u^2 \cdot 2b \\ m_0 = u \cdot 2b \cdot h \cdot C \\ \dfrac{d(u \cdot 2b \cdot h)}{ds} = \alpha_{plumes} \cdot u \cdot (2h + 2b) \end{cases}$$

One additional equation is needed to describe the assumed trajectory parallel to the bottom:

$$\cos(\omega) = \frac{dx}{ds} \qquad\qquad\qquad (28)$$

The schematization of the plume in the second part of the modeling yields one problem that can be solved in different ways. The available equations are four, whereas the total number of unknowns is five (*x, u, b, h, C*), which requires one more equation to close the system. The adopted solution implies the strong hypothesis of a linear relationship between *h* and *s,* allowing us to add the following equation:

$$\frac{dh}{ds} = k^* \qquad\qquad\qquad (29)$$

Where:

k^* is a coefficient estimated during our laboratory experiments (ranging from -0.03 to 0.24)

4.2.6 Solution of governing equations

Also in the intermediate field modeling one set of ODE is obtained, and they are solved using finite differences, in the same manner as described above for the near field. The following equations are solved for the main unknowns:

$$C_{i+1} = \frac{1}{\left[\frac{1}{C_i} + \frac{\Delta s \cdot \alpha_{plume} \cdot u_i \cdot (2h_i + 2b_i)}{m_0} \right]} \qquad\qquad\qquad (30)$$

$$u_{i+1} = C_{i+1} \cdot \left[\frac{u_i}{C_i} + \Delta s \cdot \left(\frac{\lambda^* \cdot k \cdot g \cdot \sin(\omega)}{\rho_a \cdot u_i} - \frac{C_D \cdot u_i}{h_i \cdot C_i} \right) \right] \tag{31}$$

$$h_{i+1} = h_i + k^* \cdot \Delta s \tag{32}$$

$$b_{i+1} = b_i \cdot \frac{u_i \cdot h_i \cdot C_i}{u_{i+1} \cdot h_{i+1} \cdot C_{i+1}} \tag{33}$$

All the equations developed for the near and intermediate field are implemented and solved in the Matlab software.

4.3 Model verification, sensitivity analysis, and calibration

4.3.1 Model verification

Model verification was conducted following internal coherence criteria, for example, increasing volume flow should extend the near field zone (*i.e.* stronger influence of initial conditions); increasing density of ambient water should reduce dilution at any point; and increasing diameter should enhance lateral spreading. A visual inspection based on Matlab plots was conducted, verifying that the model behaves as expected with regard to the aforementioned parameter changes.

4.3.2 Sensitivity analysis

The aim of the sensitivity analysis was to find the parameters that the model exhibits greatest sensitivity towards in order to facilitate calibration and assess the robustness of the model. Starting with a specific initial value for each parameter studied, an interval of variation in this value of $\pm$ 50 % is then applied, keeping all other parameter values constant. In Table 1 are all parameter values used summarized. Is important to remember that parameters are investigated here for which a vast literature

Table 1 Sensitivity analysis with respect to model parameter values

Parameter	Initial value	plus 50%	minus 50%
α-jet	0,0535	0,08025	0,02675
α-plume	0,0833	0,12495	0,04165
k	0,537	0,8055	0,2685
k *	0,1	0,15	0,05
λ	1,2	1,8	0,6
λ *	1	1,5	0,5
Cd	0,01	0,015	0,005

is available, but the calibration will be limited to small variations with respect to "accepted" values.

A particular case in the sensitivity analysis included the calculation step size Δs, which was analyzed for values ranging from 0.1 to 0.00001 m, looking for a compromise between computational time and accuracy (and stability). A good accuracy was found for values less than 0.01 m in the cases studied.

The greatest sensitivities were found towards α_{plume} , λ, and C_D; both regarding the measured lateral spreading b and the concentration C. Less sensitivity was noted for k and k^*, with more influence on the lateral spreading than on the concentration. As examples, figure 7 displays the results of the sensitivity analysis for α_{plume}.

The drag coefficient, in the range investigated (around 0.1 or less) is not affecting the measured properties and also variations in α_{jet}, as pointed out by Sanchez (2009), seem to have limited effects.
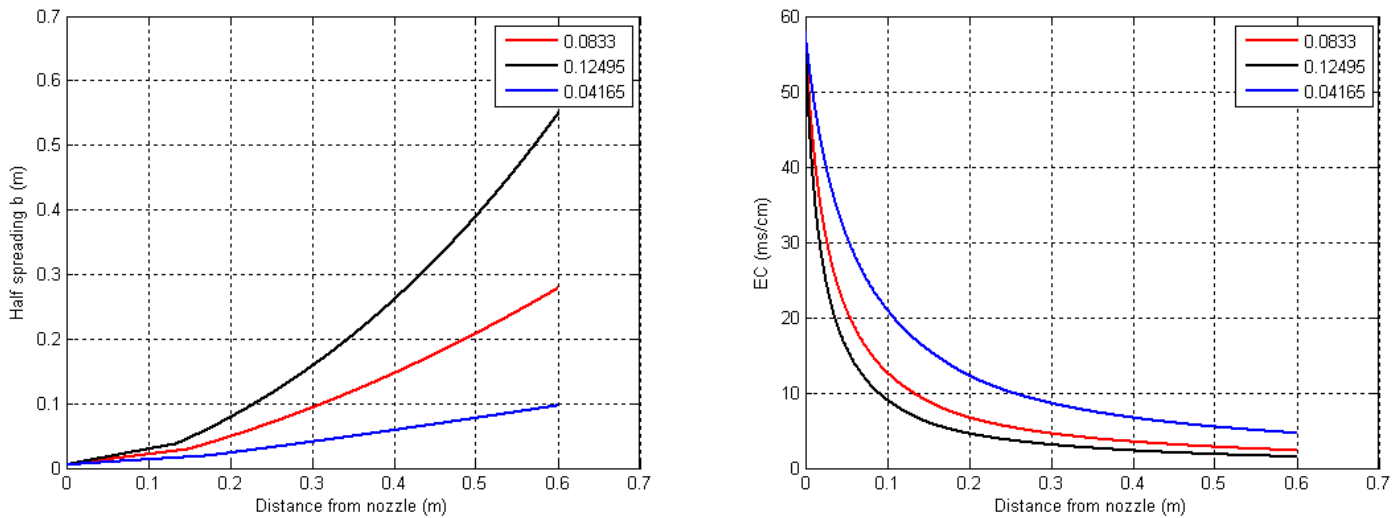
Figure 7 Sensitivity analysis for parameter α_{plume}

Calibration was based on data collected at the TVRL laboratory, as described in chapter 5.

Table 4 Parameter calibration range	
Parameter	**Range**
α-jet	0,0535
α-plume	0,1200
k	0,6370
k *	0,1300
λ	1,2000
λ *	1,0000
Cd	0,0100

Table 3 Calibrated parameters, Sb = 0	
Parameter	**Range**
α-jet	0,0535±0,03
α-plume	0,0833±0,03
k	0,537±0,1
k *	0±0,2
λ	1,200
λ *	1,000
Cd	0,010

Table 2 Calibrated parameters, Sb = 0	
Parameter	**Range**
α-jet	0,0700
α-plume	0,0600
k	0,5370
k *	0,0900
λ	1,2000
λ *	1,0000
Cd	0,0100

29

Two calibrations for this model were performed: one for all the experiments where the bottom is flat and one for all the experiments with a bottom slope different than zero. This decision was made based on the significant difference in behavior observed in experiment between these two types of conditions.

The model is physically based, and this is the reason why calibration should not play a key role for the behavior of the variables employed and studied. Some of the parameters (such as C_D, λ^*, and λ) were kept constant based on values from the literature; other parameters (k and k^*) have a expected interval of variation, because they are new parameters, introduced specifically in this model and supported only by our laboratory measurements. Values on *α-jet/plume* were suggested by Fisher (1976), but intervals of variation are expected from ± 0.0025 to ± 0.03, respectively.

4.3.4   Validation

Validation of the model, that is, the test of the model itself on a data set different from the one used in the calibration, is reported on in chapter 6 "Comparison between model simulation and data", after the presentation of laboratory experiments.

5   Laboratory experiment

A set of experimental cases were run in the Water Resources Engineering (TVRL) laboratory, in order to simulate the discharge of brine water as a negatively buoyant jet. The experimental setup, described in this chapter, is analogous to what was presented by Cipollina *et al* (2005), who described the main properties of inclined dense submerged jets.

5.1   Materials

The experimental setup developed in order to create a bench-scale submerged jet is described first. A tank situated above the main apparatus was connected using a plastic hose to a nozzle, which was located inside a larger water tank. Between them a valve was utilized to regulate the flow and a flow meter was employed to determine the flow values. Downstream the flow meter, another hose was connected to the principal one in order to leave an exit route for the air entrapped in the system before each experimental run. Also, this hose was equipped with a valve.

Summarizing, the components of the experimental system were:

- ➢ Tanks
- ➢ Flow meter and frequency meter
- ➢ Pump
- ➢ Hoses
- ➢ Valves
- ➢ Nozzles and support
- ➢ Salt
- ➢ Tracer
- ➢ Conductivity meter

5.1.1   Tanks

Tanks used in the experimental runs were:

- ➢ One medium-size plastic tank of 90 l, used to mix salt, tap water, and tracer, in order to obtain a dense effluent.

➢ One small plastic tank of about 50 l, situated above the main tank at *ΔH* (m) approximately 1 m above. This tank was filled with the dense effluent, including the tracer, and the height *ΔH* induced a flow Q from this tank to the main tank through the nozzle.

➢ Two main tanks, made of glass, originally used as fish aquariums. Average capacity of these tanks was 500 − 600 l and they were equal in all dimensions except for the length. In fact, during the experimental runs in some case interaction of the dense effluent with the wall and resulting rebound effects were observed. With a longer tank this effect, which disturbed the measurements, was delayed in time. In figure 8 is the main tank and the effluent tank shown.
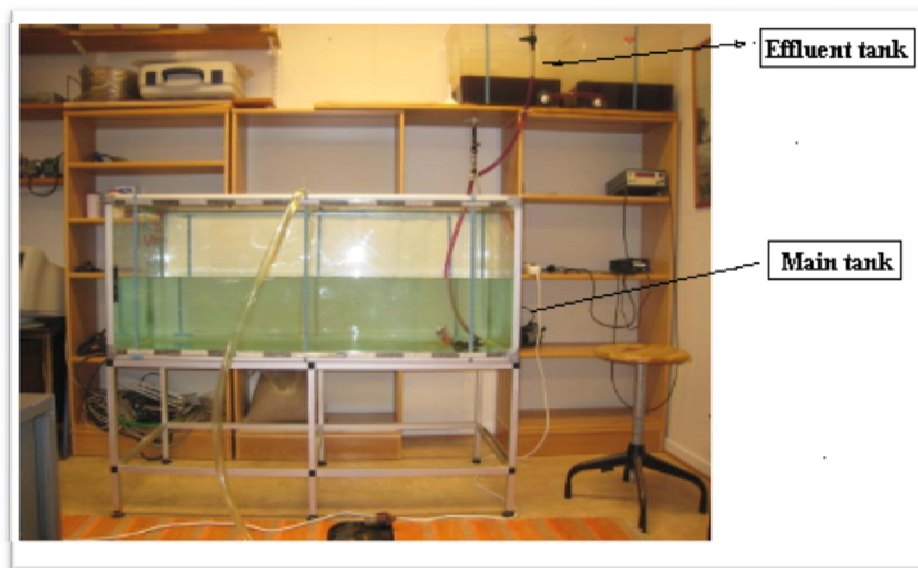
Figure 8 Water tanks used in the experiment

5.1.2 Flow meter and frequency meter

A flow meter was used to measure the quantity of flow in the hose between the high-position tanks and the nozzle. The flow meter needed a frequency meter, which was connected using an electronic circuit, specifically developed. The frequency recorded is proportional to the flow passing through the hose. The measurement system was tested before starting the experiments, as reported in the following chapters.

5.1.3 Pump

A submerged pump was used to empty the water in the main tank after an experimental run, since the tank has no outlet. The maximum declared pump flow was 3600 l/h; therefore around 12 minutes was

needed to empty all the water in the smaller main tank and 16 minutes in the larger one. The pump was also used to lift the saline water, prepared in the plastic tank, to the high-elevation tank.

5.1.4 Hoses and valves

A 15 mm diameter plastic hose was used to connect the high elevation tank with the nozzle, including the circuit to remove the air from the pipe. Another hose, which was 25 mm in diameter, was connected to the tap during filling and emptying of the main tank.

Two gate valves were used in the experimental apparatus. One was situated on the hose connecting the effluent tank with the nozzle in order to regulate the flow. The second one was situated further downstream, after the flow meter, and was connected to a hose which was open to the atmosphere at the other end. When both the valves were opened and the nozzle was manually obstructed, the air entrapped in the main hose was bubbling and released through the open end of the second hose. This operation was necessary, prior to each run, or air would affect the flow. The two valves are shown in figure 9.
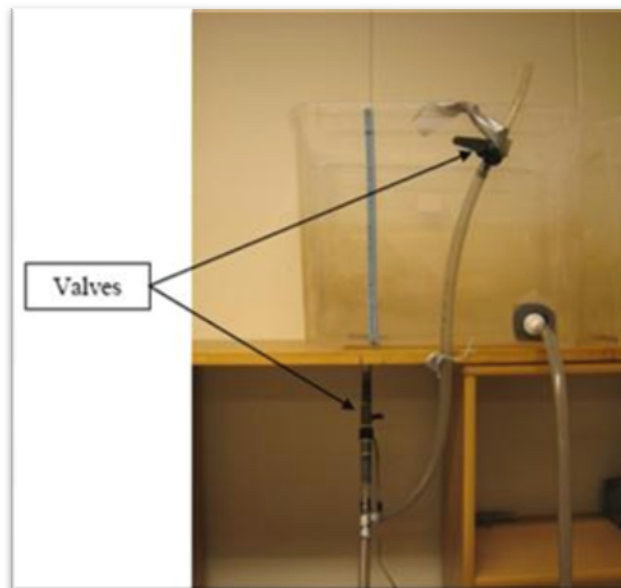
Figure 9 Valves system in the experimental apparatus

5.1.5 Nozzles and nozzles support

Saline dense water was injected in the main tank, filled with tap water through a nozzle. The nozzle was mounted on a special support (see figure 10), which allowed us to change the initial direction of the jet, applying different angles Θ from the horizontal plane. The support was easily fixed and

removed from the glass bottom of the main tanks through suction pads applied on the bottom. The nozzle diameters used in the experimental set up were:

- ➢ 2,3 mm
- ➢ 3,3 mm
- ➢ 4,8 mm

Figure 10 Nozzle support arrangement

5.1.6 Salt and tracer

Simple Sodium Chloride (NaCl) was added to the tap water in order to create the dense effluent. Different concentrations were used, including 4 %, 6%, and 8%, expressed in salinity percentage (1% equals 10000 ppm).

Potassium permanganate was added to the dense effluent in order to change the color of the saline water in the discharged jet. The tracer converted the transparent water into a purple color. The use of a purple jet was made to facilitate the observation of the behavior of the jet in the main tank with fresh water. The concentration of the tracer was initially 0.1 g/l.

5.1.7 Conductivity meter

The conductivity meter was an essential instrument in the experiment; through the measurement of the electrical conductivity, and knowing the conductivity of the effluent and fresh water, it was possible to obtain a direct measure of the salinity and indirectly of the dilution and mixing in each point of the jet /

plume. The conductivity meter used was a portable device LF 530, equipped with temperature correction of the measurements.

5.2 Procedure

5.2.1 Preliminary measurements

Preliminary measurements were conducted in order to obtain reference data and to check if our measurement tools (*i.e.* flow meter, conductivity meter) were reliable and coherent with literature data. These measurements are divided in:

➢ Measurements of salinity, density, and conductivity, performed with simple tools like the cited conductivity meter and a laboratory balance, gave us information about water density and conductivity variation as a function of salinity at a constant room temperature of 20 ° C ±1 ° C. The results are plotted in figure 11
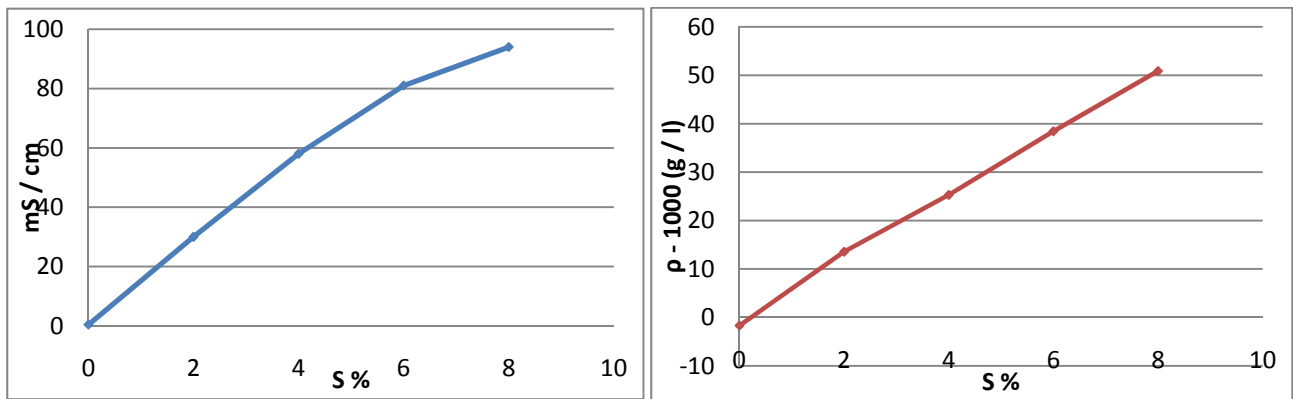
Figure 11 EC variation with salinity level (left side) and density variation with salinity level (right side)

Each experimental run was characterized by a set of parameters, and the first step of each run was to choose the combination of parameter values. The parameters of interest were:

➢ Diameter of nozzle **ϕ** (4.8; 3.3; 2.3 mm)

➢ Initial jet angle **Θ** to the horizontal line (0; 30°)

➢ Bottom slope **Sb** (0; 15 %)

➢ Salinity of brine discharge **S** (4; 6; 8 %)

Two experimental runs could be performed using the same volume of fresh water in the main tank; subsequently, the water in the main tank had to be replaced. First, a low velocity was employed to avoid a large quantity of tracer in the main tank. The results from the low-velocity run were obtained;

then the velocity was increased to record data for a jet with higher initial velocity. This procedure was used to obtain data for two different jets without replacing the water in the main tank.

Each run was about 60 to 130 seconds long, and a set of measurements were collected according to:

➢ Measurement of flow: continuous recording with the frequency meter;
➢ Measurement of lateral spreading: recorded the lateral width of the flow at 3 measurement points, at an axial distance from the nozzle of 0.2, 0.4, and 0.6 m. The technique employed to collect the data consisted of drawing lines directly on the bottom glass of the tank showing the borders of the jet;
➢ Measurement of electrical conductivity: recorded on the jet axis at the same distances cited above, both during the run and 30 s after the run was stopped;
➢ Measurement of thickness (*i.e.* the vertical spreading): measured at the same points, 30 s after the run was stopped, in order to avoid the influence of the initial momentum jet;
➢ Additional measurements: for example, water and tracer temperature, and conductivity. These variables are necessary to record in order to correct sampled data.
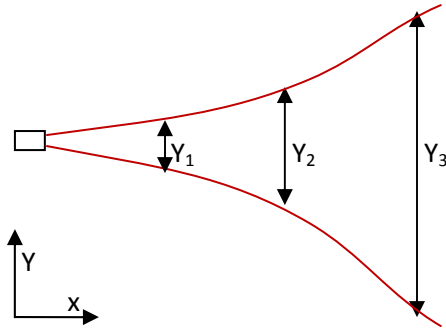
Figure 12 Plan view of lateral spreading measurements along the flow

5.3   Observations
The experimental data are reported in the appendix.

5.3.1   Data analysis
Spreading data collected for the parameter values described above were analyzed in order to establish the effects of these parameters and, eventually, correlate them using non-dimensional numbers like the densimetric Froude or Reynolds numbers.

5.3.2 Parameter variation effects on lateral spreading

In this section are the effects of geometrical characteristics of the submerged discharge (*i.e.* Θ and Sb) on the lateral spreading of the dense effluent discussed. Spreading data are reported normalized with the nozzle diameter, in order to homogenize different test conditions on a common scale. The combinations of parameter values taken into account and analyzed are reported in table 5.

Table 5 Set of geometrical parameter combinations studied

Θ = 0°	Θ = 30°
Sb = 0 %	Sb = 0 %
Θ = 0°	Θ = 30°
Sb = 15 %	Sb = 15 %

The normalized spreading (y/D vs x/D) is initially plotted in graphs for constant salinity of effluent S and constant nozzle diameter D, creating a set of point for each combination of geometrical parameters. In this way one graph is showing experimental cases homogeneous between them and therefore comparable.

This first step allows us to visually understand the effect of each single parameter, with the main goal to distinguish between positive and negative effects regarding the mixing, *i.e.* increasing or decreasing spreading, respectively.

Two typical graphs obtained in this way (figure 13 and 14) are shown here. The figures seem to show that nozzle inclination Θ has a negative effect on spreading in the area under observation, while Sb has a strong positive one. The combined effect, with our set of parameter values, seems to be positive.
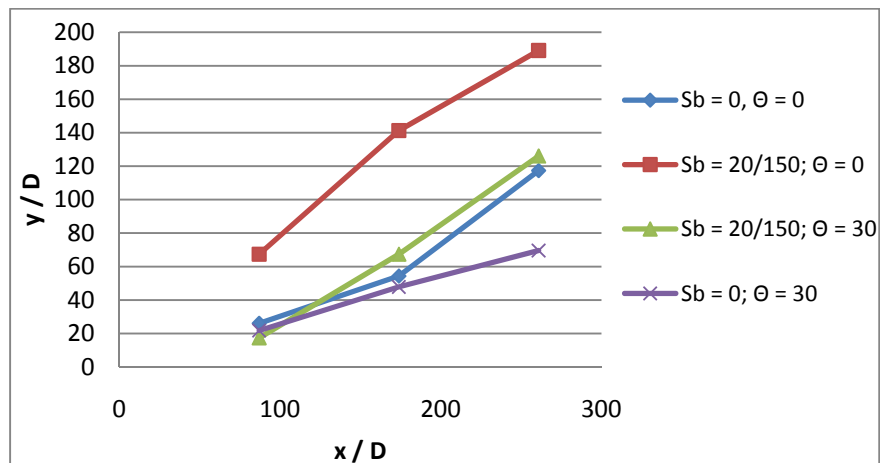
Figure 13 Effects of geometrical parameters on lateral spreading; S = 4 %; φ = 2.3 mm
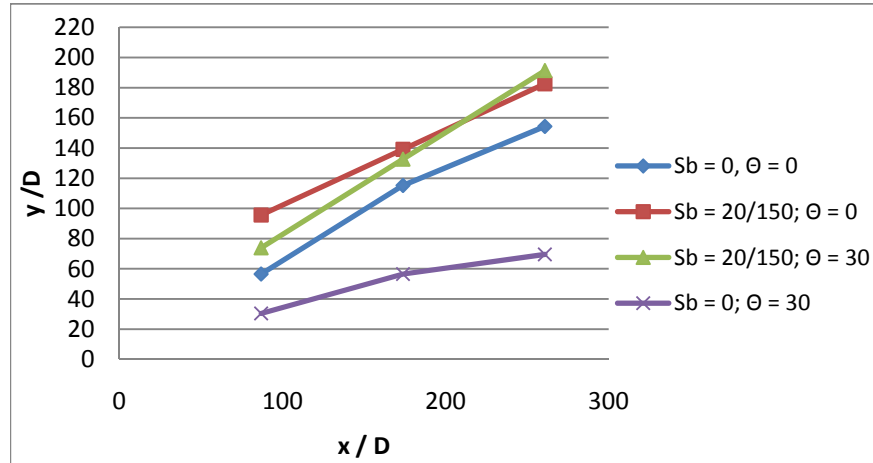
Figure 14 Effects of geometrical parameters on lateral spreading; S = 4 %; φ = 2.3 mm

Furthermore, all effects were quantified with the following procedure. For each experimental run the change in normalized spreading with respect to the case in which parameter values are set to 0 (respectively $\Theta = 0°$; Sb = 0 %) was calculated. Change in normalized spreading, recalling that we have 3 measurements points will be:

$$\Delta\frac{Y_i}{D} = \left(\frac{Y_{i,k}}{D}\right) - \left(\frac{Y_{i,0}}{D}\right)$$

Where:

$Y_{i,k}$ is spreading measured in i-th measurement point with k-th set of parameters.

If k equals zero that means that both $\Theta = 0°$; Sb = 0 %. In this case the unit of measurement of the calculation will be the number of diameters.

A map of all these comparisons is presented in the appendix. It can also be observed how the visual information described above is confirmed by actual data, with a few exceptions.

Mean value of change in spreading for all runs and measurement points are: increase by 28 diameters for the single effect of bottom slope; decrease by 18.8 diameters for the single effect of nozzle inclination; and increase by 10.5 diameters for the combined effect.

5.3.3 Reynolds number analysis

The data were investigated so see whether any relationship existed between *y/D* and the Reynolds number. All experiments show values of the Reynolds number greater than 2000, so there was no need to distinguish between turbulent and laminar conditions (all cases were assumed turbulent).

In the first type of analysis, *Yi/D* with the same diameter was plotted versus the Reynolds number, and a check was made if there was any linear correlation. Very low values of R^2 are obtained for all cases, as shown in figure 15.
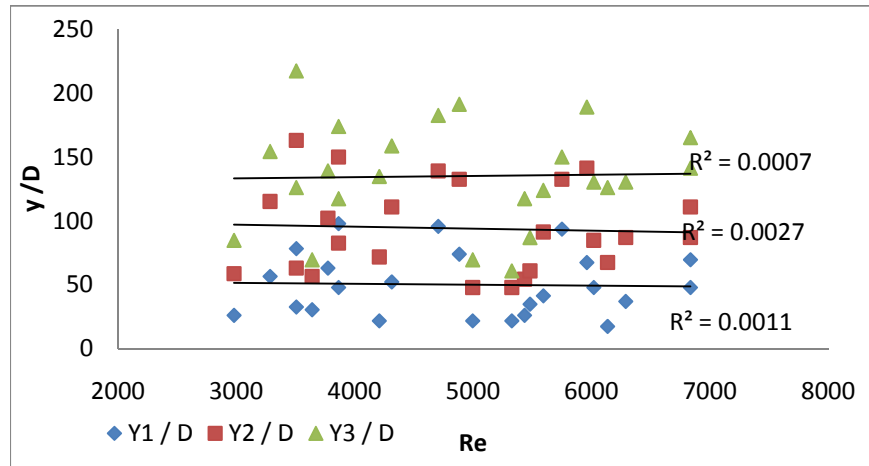
Figure 15 Non-dimensional spreading (Yi/D) versus the Reynolds number, D=2.3 mm

The second type of analysis involved plotting the non-dimensional spreading *Y/D* versus *x/D* for each class of Reynolds number available and taking other geometrical parameters as constant. Classes of Reynolds number available ranged from 2000 to 7000.

Previous investigations encompassing plane submerged jets showed how increasing Reynolds numbers produced decreasing lateral spreading (Suresh *et al.,* 2008). In this study, even if there was a limited range of Reynolds numbers available, an attempt was made to discover a similar effect, as shown in figure 17, which is representative of all the experimental data with Θ =0 and Sb = 15 %. All Reynolds number classes with less than 4 values were neglected in the analysis. A linear tendency was found for the highest and lowest Reynolds number classes. Spreading is effectively limited by increasing Reynolds number, but the differences are not as evident as in Suresh *et al*. data.
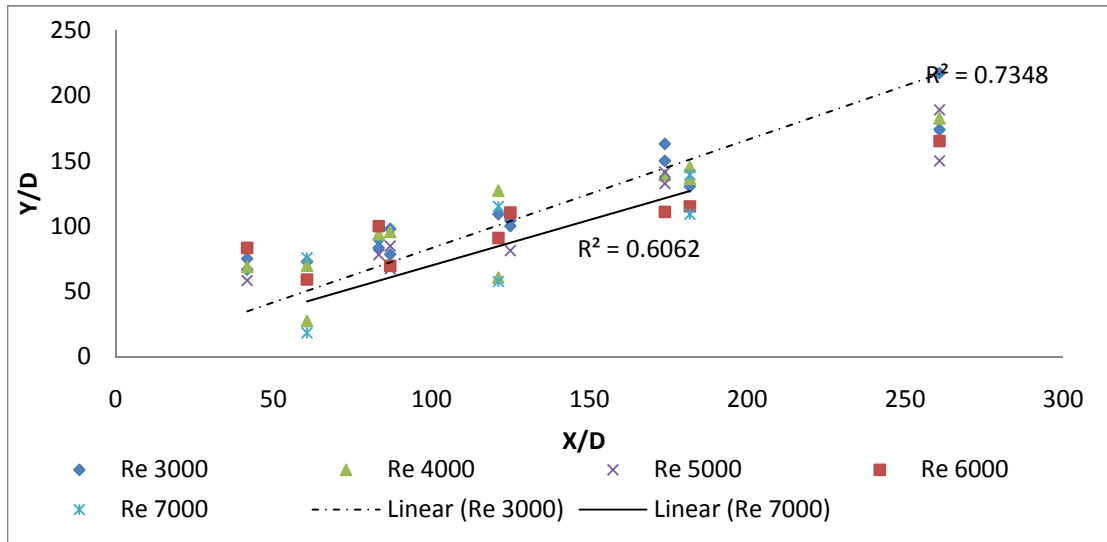
Figure 17 Non-dimensional spreading (Yi/D) for all Reynolds classes

5.3.4 Densimetric Froude number analysis

Figures were plotted with y_1/D, y_2/D, and y_3/D versus the densimetric Froude number to explore any relationships. The different parameters of interest are the diameter (D), the salinity (S), the angle of the nozzle (θ), and the bottom slope (Sb). Three of those parameters were fixed in the analysis, leaving one free, and the correlation coefficient (R^2) was calculated to check if any linear relationship was present.

Is important to underline that points x_1, x_2, and x_3 of measurement were arbitrarily chosen at a distance of 0.2, 0.4, and 0.6 m, respectively, from the nozzle and these points do not have any intrinsic physical meaning, as, for example, the maximum jet height or impact point, used in the analysis by Cipollina *et al.* (2005). This condition suggests that any possible correlation might be found in combination of parameters in which diameters (D) are fixed, so much that x_i/D would be comparable between experimental cases.

The overall value for the R^2-coefficient is found to be low, with a value of 0.34, whereas the highest values are found for y_2/D and y_3/D versus the densimetric Froude number, with Sb, S, and φ fixed, as shown in tables 6 and 7.

Table 6 Correlation coefficients for y2/D versus densimetric Froude number with salinity, nozzle diameter, and bottom slope fixed

Sb = 15 %	y2/D			
S/φ	0.0023	0.0033	0.0048	Average
4	0,1257	0,2162	0,6605	0,3341
6	0,8258	0,2023	0,7734	0,6005
8	0,4185	0,8529	0,9810	0,7508
Average	0,4567	0,4238	0,8050	0,5618

Other types of correlation were tried, in order to overcome the lack of physical meaning of measurement point locations. For each run, a linear regression was calculated between y_i/D and x_i/D, obtaining the parameters of slope (m) and intercept (b). The parameter values described above were then analyzed again, using m and b instead of y_i/D (correlation against densimetric Froude number).

Table 7 Correlation coefficients for y3/D versus densimetric Froude number with salinity, nozzle diameter, and bottom slope fixed

Sb = 15 %	y3/D			
S/φ	0.0023	0.0033	0.0048	Average
4	0,1934	0,8838	0,9476	0,6749
6	0,7579	0,2472	0,3099	0,4383
8	0,8885	0,7842	0,4162	0,6963
Average	0,6133	0,6384	0,5579	0,6032

The overall R^2-coefficient was found to be 0.41, generally higher for correlation regarding m than b. The best results for both these parameters were found when Sb, S, and Θ were fixed, as reported in table 8 and graphical examples are given in figures 18 and 19.

Table 8 shows the result of the linear regression for m when the bottom slope is 15 %, nozzle inclination is 30°, and the salinity takes on three different values (4%, 6%, and 8%). In the same table is also the linear regression for m when the salinity is 4 %, nozzle inclination is 30°, and the bottom slope takes on two different values (0 and 15 %) shown.

Table 8 Correlation coefficient for m (left) and b (right) versus densimetric Froude number with bottom slope, salinity, and nozzle inclination fixed at 30°

S/Sb	0	15	Average	S/Sb	0	15	Average
4	0,8073	0,8917	0,8495	4	0,0052	0,5799	0,2925
6	0,8830	0,8943	0,8887	6	0,1281	0,9179	0,5230
8	0,8110	0,7605	0,7857	8	0,4898	0,9303	0,7101
Average	0,8338	0,8488	0,8413	Average	0,2077	0,8093	0,5085
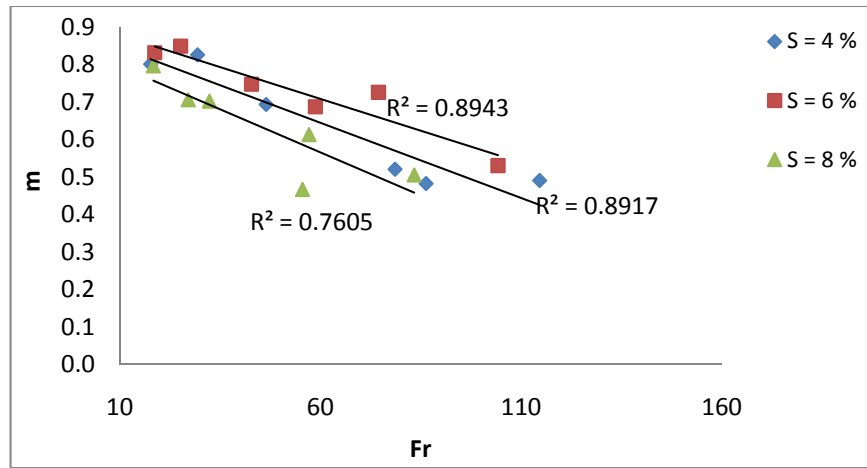
Figure 18 Slope linear correlation coefficient m versus densimetric Froude number (Θ = 30° and Sb = 15 %).
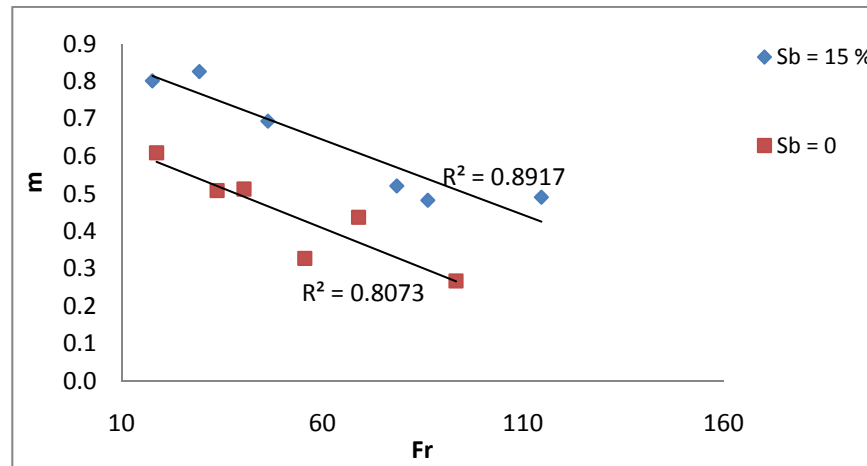
Figure 19 Slope linear correlation coefficient m versus densimetric Froude number (Θ = 30° and S = 4 %).

6 Comparison between model simulation and data

6.1 Validation of the model

The validation of the model represents one of the most important phases in the model building sequence, and for this reason it is necessary to use a completely independent set of data from the one used during the calibration. The validation procedure requires some definitions, taking into account different kind of errors. For each experimental run, these errors are defined as:

$$\varepsilon_{EC,i} = \left| \frac{EC_{model,i} - EC_{experimental,i}}{EC_{experimental,i}} \right|$$

$$\varepsilon_{b,i} = \left| \frac{b_{model,i} - b_{experimental,i}}{b_{experimental,i}} \right|$$

$$\varepsilon_i = \frac{\varepsilon_{EC,i} + \varepsilon_{b,i}}{2}$$

where:

$\varepsilon_{EC,i}$ is the error estimated in the modeling of electrical conductivity (EC), in the i-th point of the measurements (i = 0.2; 0.4; 0.6 m)

$\varepsilon_{b,i}$ is the error in modeling the lateral spreading b, in the i-th point of the measurements

ε is the overall error, in the i-th point of the measurements

The validation process was carried out considering the two different cases with and without bottom slope separately, as was done for the calibration.
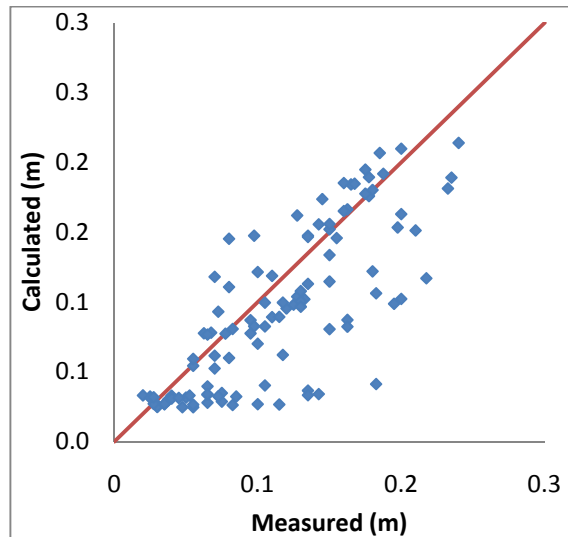
Figure 20 Evaluation of the error between measured and calculated values for the half spreading
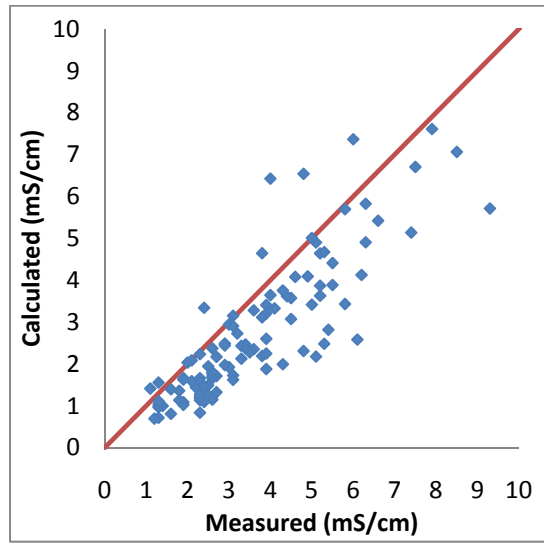
Figure 21 Evaluation of the error between measured and calculated values for the Electrical Conductivity (EC)

In figures 20 and 21 are graphically illustrated the error resulting from the modeling of the half spreading and the concentration for the tests without the bottom slope. The best results are for the values closer to the red straight line, which corresponds to perfect agreement between the model calculations and the measurements. The sum of these two errors obtained in the modeling is used to estimate an average error. The same procedure, omitted here, was done for the other case of study. In the appendix are also two examples of the model output, compared with the measured data, reported.

The average overall errors for the two calibrations of parameter values (with and without bottom slope) were found to be, respectively, 37% and 29%. Thus, the model can be considered as properly validated, especially for flat-bottom conditions.

6.2 Errors characteristics and discussion

In this chapter some characteristics of the errors are discussed, treating the two calibrated models simultaneously.

6.2.1 Electrical conductivity (EC) comparison

The average error in the modeling of electrical conductivity (EC) was found to be 0.33. Most of the errors (30% of the total) are concentrated in the interval $0.2 < \varepsilon < 0.3$, and 18% of the error are lower than 0.2, which was considered by Sanchez (2009) as a target threshold for accuracy. Visual results of this analysis are reported in figure 22.
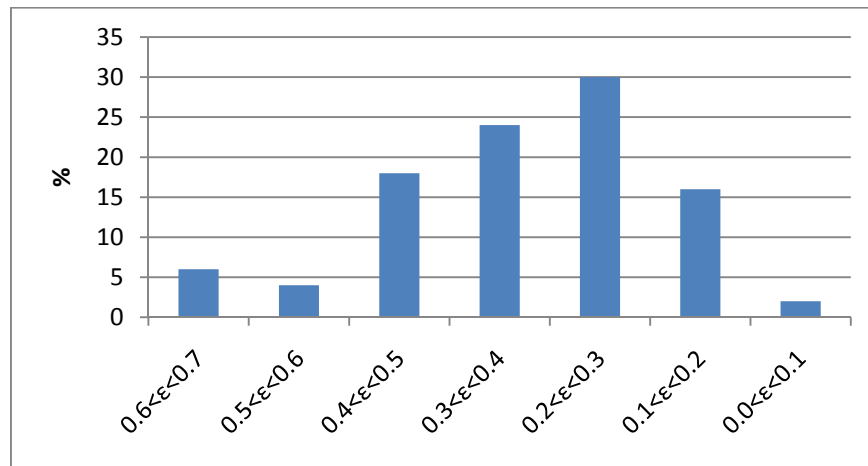
Figure 22 Distribution of simulation errors in EC modeling

6.2.2 Lateral spreading width (b) comparison

Average error in the modeling of lateral half spreading (b) was found to be 0.29. Most of the errors also in this case (40% of the total) are concentrated in the interval $0.2<\varepsilon<0.3$, and 18% of the error are lower than 0.2. No errors greater than 0.5 were found.
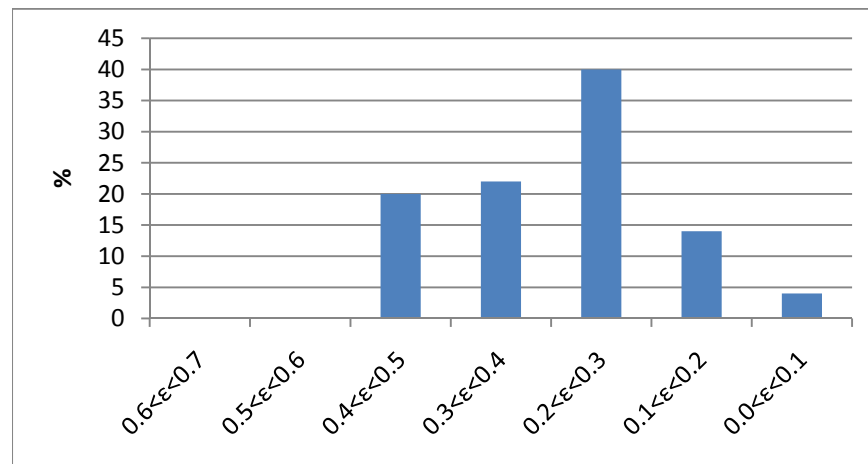
Figure 23 Distribution of simulation errors in spreading half width (b) modeling

6.2.3 Errors and geometrical characteristics relationship

An investigation of the other error characteristics was also performed. The goal was to investigate if some geometrical parameters are more likely to produce errors in the simulation, for example, the model can fail to describe small diameters or high salinities.

As cited in the previous chapter, bottom slope is very effective in this respect, even if a different calibration was tried specifically for the employed slope of 7.66°. Error for the simulations with bottom slope was in average 0.37, while without it was 0.28.

Another effective parameter is the salinity (S). When salinity takes on the values 4, 6, and 8%, the average error is increasing with the corresponding values of 0.25, 0.28, and 0.35, respectively.

Discharge angle with the horizontal line (Θ) and diameter (D) of the nozzle have little effect in the intermediate zone, even if experiments with the smallest diameter produced a slightly larger error.

6.2.4 Errors and non-dimensional numbers

Possible relationships between the model errors and Reynolds or densimetric Froude numbers were investigated, in order to understand if there are some intervals of variation of these numbers which induce larger errors. Electrical conductivity errors and spreading errors were analyzed separately.

The correlation coefficient when a trend line is fitted is, in each case, too small to establish any relationships between the error and the Froude/Reynolds numbers in order to determine whether there is any range of numbers where the error is larger. It is possible to identify large errors for any range of
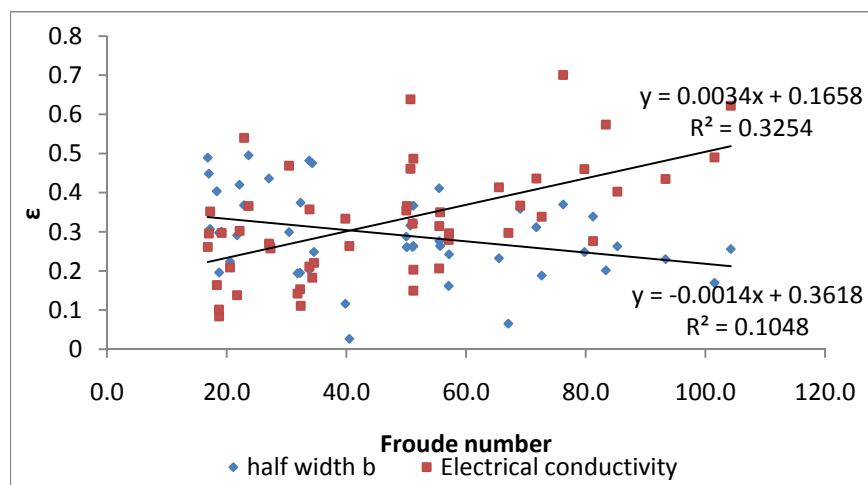
Figure 24 Simulation error versus densimetric Froude number

numbers, as illustrated by figures 24 and 25.
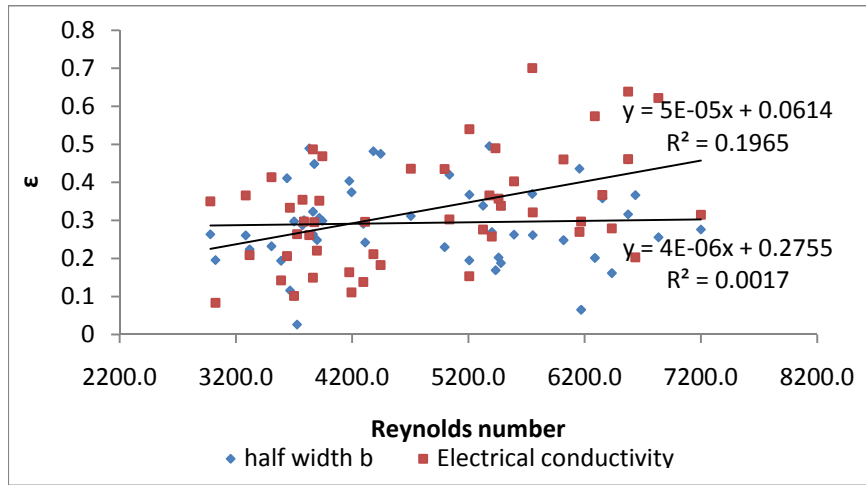
Figure 25 Simulation error versus Reynolds number

7 CORMIX® simulation
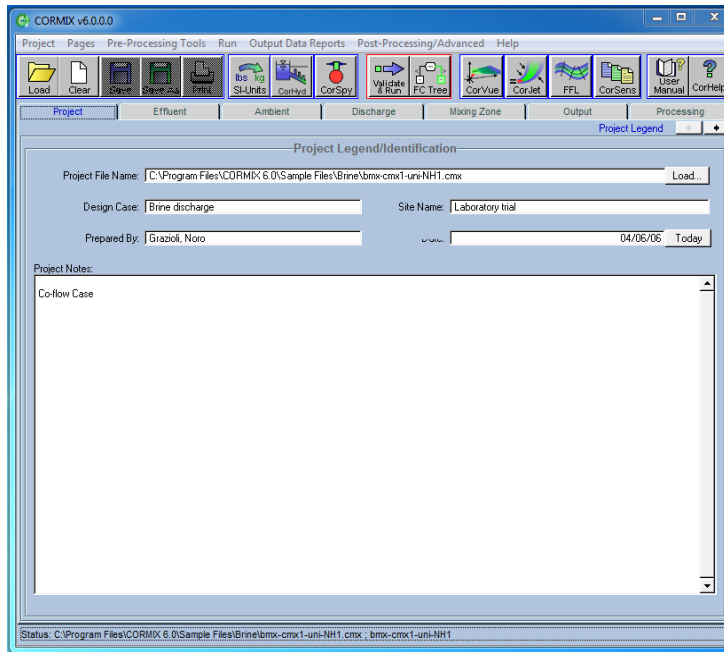
Figure 26 CORMIX Main Project menu

CORMIX® (Cornell Mixing Zone Expert System) is a well-known software for hydrodynamics modeling utilized by USEPA as a decision support system for environmental impact assessment. The program is used for planning and describes the near-field and far-field discharges with superficial or submerged diffusers. The purpose of the modeling with CORMIX® was to simulate the processes involved in the laboratory experiment in order to compare the experimental results with the data obtained from the mathematical simulations.

The program is user friendly thanks to its graphical user interface (figure 26) that lets the operator introduce all the parameter values necessary for the case studied. The input data needed are all grouped under six tabs: Project, Effluent, Ambient, Discharge, Mixing zone, and Output. The last tab named "processing" is the only one that is not requiring input data and is used only for running the simulation. The first things to define it are the name of the project, the design case, and all the information that permits to easily label the project for later use.

The second tab named "Effluent", shown in figure 27, allows the user to specify the characteristics of the effluent. The discharge type also defines what the subsequent values needed to obtain the simulation are. For example, choosing a conservative pollutant as effluent instead of brine, influences all the following tabs, due to the hydrodynamic assumptions made by the software. In a brine discharge, as in the present case, the user is asked to enter alternatively the velocity or the flow rate of the effluent, and the density of the brine. To assist in the calculation of the effluent density a simple tool within CORMIX® can be used to obtain the correct value just entering the temperature of the effluent and the salinity as parts per thousand, which are approximately grams of salt per kilogram of solution.
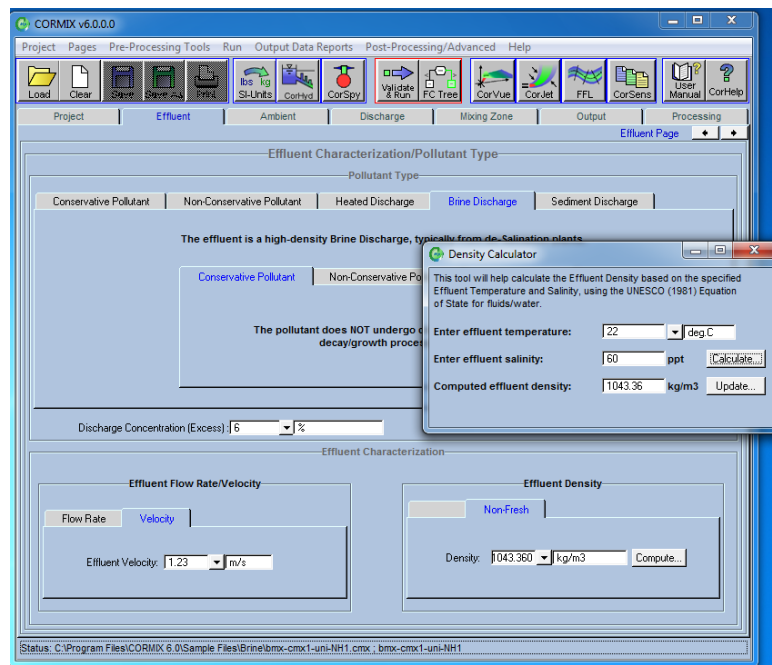
Figure 27 Effluent characteristics and density calculation

After defining the effluent characteristics, the next step is to set the "Ambient" conditions in the proximity of the discharge point. The software schematizes the receiving water (ambient) using a rectangular cross-section, and this simplification can require some further considerations in the case of highly irregular water body sections, but for our purposes it was not a limitation due to the simple geometry of the tank. An example of the characteristic lengths used for the receiving water schematization is shown in figure 28.
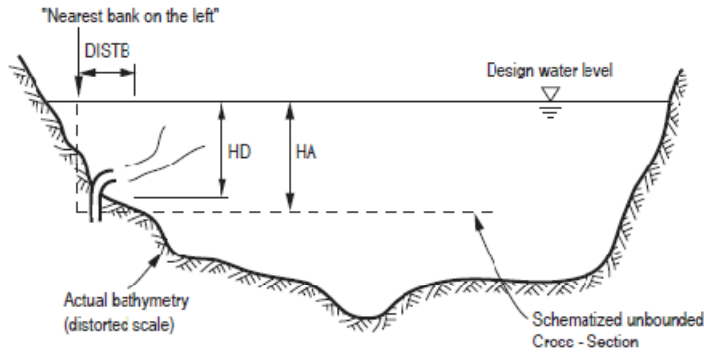
Figure 28 Example of a jet discharge in an unbounded cross section (Doneker and Jirka, 2007)

For the brine discharge the software automatically defines the conditions as being unbounded and considers one of the banks to be close to the discharge point, whereas the other bank is far away from the emission point.

Another simplification introduced when modeling the mixing of the brine is the ambient steady state condition. This assumption, usually adequate, is necessary to describe the mixing processes even though it is never exactly true since "the mixing processes are quite rapid relative to the time scale of hydrographic variations" as stated by Doneker and Jirka, (2007).

The influence of the ambient parameters was negligible in our tests considering the absence of wind or ambient currents during the simulation in the laboratory.

The CORMIX® software is a powerful tool to simulate large-scale cases in the field; however, it is more difficult is to reproduce small-scale situations like the ones that are present during a laboratory experiment. The first difficulty encountered in the present application was to introduce the bottom slope in the CORMIX® simulation. To obtain the depth at the discharge point, the software uses a simple equation (34), and this formula may be useful in a field case because the discharge occur at a certain distance from the bank, and knowing the bottom slope it is easy to obtain the discharge depth. In our case, where the discharge occurred at the upstream end of the tank, it was not possible to enter the real value of the parameter DISTB. Instead, we were forced to enter an arbitrary value to obtain the correct depth at discharge point. The same applies for the case with the horizontal bottom; moreover, in this situation one have to introduce a nearshore slope just to obtain the depth at the discharge point, and subsequently an offshore slope that must be put equal to 0.

$$HD = DISTB \cdot tan\,(slope) \tag{34}$$
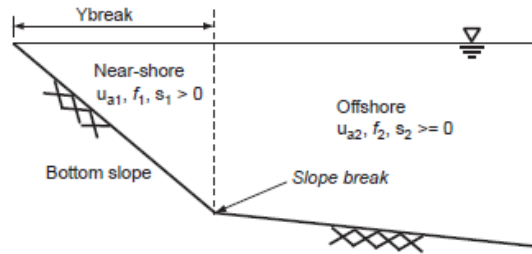
Unbounded Cross-section for Brine/Sediment Effluents

1. Bounded laterally on one side only
2. Uniform ambient near-shore current field u_{a1} = constant$_1$; u_{a2} = constant$_2$
3. Positve near-shore slope s_1 with break to offshore slope s_2 at distance Ybreak
4. Near-shore Darcy friction factor f_1; offshore Darcy friction factor f_2
5. Uniform channel in downstream direction

Figure 29 Geometrical characteristics of the model (Doneker and Jirka, 2007)

Another parameter requested is the Darcy-Weisbach coefficient, which quantifies the frictional losses caused by the water flowing over a bed. It was set to 0.01, the lowest value accepted by the software, and this choice was made considering the properties of the glass bottom.

In the discharge tab are the characteristics of the ports, or diffusers, defined (more than one can be present), the distance to the closest shoreline, and the initial horizontal and vertical angles of the jet with respect to the reference coordinate system. As stated before, the shoreline location is not a meaningful parameter for the present case, but it is just a measure used by CORMIX$^{®}$ to check the consistency of the values entered for the slope and the depth at the discharge point.

In order to insert the correct values for sigma Σ and theta Θ (defined below) it is important to look at the axis system.

- The X axis represents the ambient current direction.
- The Y axis represents bottom slope direction; as default, the direction of the effluent and the bottom slope are perpendicular.
- The Z axis orthogonal to the plane XY represents the depth of the receiving water considered.

Theta (Θ) is the vertical port angle, defined as the angle between the port centerline and a horizontal plane. As examples, the vertical angle is 90° for a discharge pointing vertically upward, and it is 0° for a horizontal discharge.

Sigma (Σ) is the angle measured counter-clockwise from the ambient current direction to the plane projection of the port center line. As examples, the horizontal angle is 0° when is parallel to Y axis and orthogonal to the bottom slope, and it is 270° when the discharge follow the slope.

Our study involves four different situations to model:

1. a bottom slope equal to zero and the nozzle parallel to the bottom,

2. a bottom slope equal to zero and the nozzle inclined 30° respect to the horizontal plane,

3. a bottom slope of 8° respect to the horizontal and the nozzle parallel to the bottom,

4. a bottom slope of 8° and the nozzle inclined 30° respect to the horizontal plane.
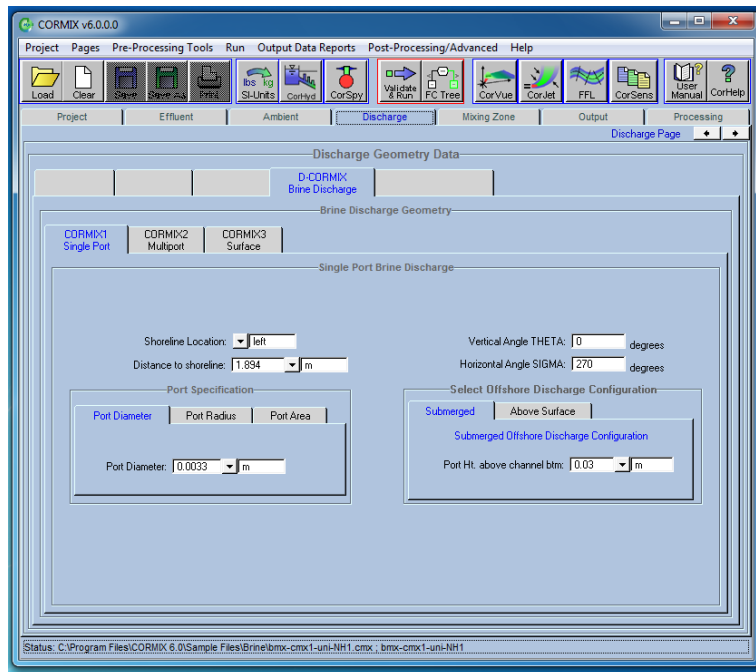
Figure 30 Discharge dialog window

The software outputs are two prediction files used by CorVue, the 3D visualization tool of CORMIX®, to build a graphic representation. The visual output was not usable due to some software glitches, nevertheless from the prediction file it was possible to extrapolate the spreading and the conductivity values and put them into a spreadsheet in order to compare the CORMIX® output with the measurements. The graphical comparisons are reported in the appendix for some cases of interest.

52

8   Discussion of results

8.1   Experimental work

The experimental setup, described in chapter 5, was easy to use and all the measurements of the jet evolution could be efficiently taken during each run. Nevertheless, the method of measurement requires some additional comments.

The measurement of the lateral spreading, recorded on the bottom glass, was strongly influenced by the visual impressions of the person who drew it, which created some difficulties to estimate the accuracy of the measurements. An alternative and more reliable methodology was applied by Cipollina *et al.* (2005) and Suresh *et al*. (2008), who used techniques based on image processing, capable of recording the jet with more accuracy, also at the lowest levels of tracer concentration.

The measurement of electrical conductivity EC through a portable device is quite fast, but brings with it uncertainties concerning the exact location of the measurement point. Also, the introduction of a probe during the test can disturb the flow regime downstream the measurement point. It was also difficult to estimate the error associated with the probe measurements.

8.2   Parameter influences

The influence of the geometrical parameters on the lateral spreading properties was presented in chapter 5.3.2. It was observed how the presence of a bottom slope (Sb) of 15 %, or 7.66° has a positive effect on the lateral spreading; increasing the spreading with 28 diameters in average (D) with respect to the case in which a bottom slope is absent. In opposite, the presence of an angle of inclination of the nozzle ($\Theta = 30°$) reduced the spreading (always an average value is given) with 18.8 diameters. The combined effect of bottom slope and nozzle inclination remains positive, with a 10.5 diameters increase.

The reduction in spreading caused by an angle of inclination of the nozzle can be explained by the fact that in this way the impact of the buoyant jet with the bottom is delayed, and it remains for a longer time in contact with ambient water. The interaction with the bottom barrier creates a compaction of the buoyant flux, which from that point can only expand laterally, increasing in this way the spreading. The later this interaction occurs, the smaller will be the lateral spreading, with other factors taken constant.

A lot of difficulties were found in explaining the increase in spreading caused by the presence of a bottom slope. No reasonable explanation was found and also the model presented in chapters 4 and 7 failed in describing this effect. More studies are required to formulate a relevant hypothesis.

8.3 Dimensional analysis

Analysis (chapter 5.3.3) showed that no linear relationship could be found between the Reynolds number and the normalized values of the lateral spreading. The R^2-coefficient values were very low, on the order of magnitude of 10^{-3}, and it can be concluded that for the range of Reynolds number studied (from 2000 to 8000) no direct influence on the normalized spreading is observed, in contrast to the results published by Suresh *et al.*(2008) for a plane jet development.

Froude number analysis was tried, with the parameter values described in chapter 5.3.4, finding correlation for each normalized spreading y_i/D with the densimetric Froude number, keeping all parameters except one constant. Low correlation was found also in this case, considering that the maximum average value of R^2 was 0.60 for y3/D, when bottom slope, salinity, and diameters were fixed and the nozzle inclination varied. Other correlations were tried (b and m parameters versus Froude) giving slightly better results, but only for the case in which salinity, bottom slope, and nozzle inclination were fixed, letting the diameter vary (the average maximum R^2 values were 0.84 and 0.51, respectively, for b and m). In these cases (see table 8), both m and b decreased with increasing densimetric Froude number.

Considering all combinations investigated, as an average, it is possible to say that low correlation was found between the lateral spreading and any non-dimensional numbers investigated.

This fact can be explained considering how both the Froude densimetric number and Reynolds number are calculated based on the initial conditions, *i.e.* they are representative of the initial state of the flow. Our study wanted to be comprehensive concerning both near-field and intermediate-field properties. The former is strongly dependent on the initial conditions, whereas the latter are no more influenced by these conditions. The absence of any correlation with the initial properties can be seen as an indication of being in the intermediate field, allowing us to use a different set of equations for the near and intermediate field, as discussed in chapter 4.

However, it was not possible in this study to propose any new criterion for identifying the location of the near field, which should be a good topic for future research. Regarding this, in the present work, the hypothesis of Christodoulou (1991) were merely applied.

8.4 Matlab model

The Matlab model showed very good behavior in modeling the experimental runs and the best results were obtained for the runs without the bottom slope, as highlighted by the lower average error calculated in chapter 6. The average error obtained in this case was around 28 %. Analyzing the experimental runs without bottom slope, an effort can be made to determine where more of the errors are found regarding the spreading and the concentration. Spreading values above the average are found for the runs with a salinity of 8 %, where an average error of 46 % was calculated. For all other salinities the average spreading error is below or slightly higher than 28 %.

With regard to the EC the error is more widely spread; above average values are found independently from the geometrical configuration or salinity used in the experimental run, but the errors are comparable with the one found for lateral spreading.

In the experimental runs with slope there are complete data available only for few runs; thus, it is more difficult to obtain firm conclusions. The first thing to notice from the comparison of the model with the experimental results is that the error for the lateral spreading is within the range of 30 % for all the measurements, slightly above the error without bottom slope. Things became different considering the Electrical Conductivity, as a matter of fact the error made in this case is definitely larger and in particular for the measurements with Θ equal to zero, where the error was around 60 %, twice the error made for Θ equal to 30°. The Matlab model in general is less accurate in predicting the values when a bottom slope is present, but in this case the error is definitely larger than expected. In discussing these results, one must be taken into account the difficulty in measuring the conductivity at the same point every time and the extreme variability in the readings obtained with the probe used.

8.5 CORMIX® software

CORMIX® was developed as software for hydrodynamic modeling of real (field) cases. In our study, the model was used to test its ability to describe results from small-scale laboratory experiments. CORMIX® behaves unexpectedly in these circumstances by providing quantitative values that are comparable with those obtained in our study, but which have no physical meaning. In this regard, it is

illustrative to compare two experimental runs, that is, runs 20 and 21. In these two runs one would expect a completely different behavior, since the only common characteristic was the diameter of the nozzle, being 4.8 mm. For run 20 there was a bottom slope of 8° and an initial angle Θ equal to 30°, whereas run 21 had no bottom slope and Θ equal to zero.. However CORMIX® merely provided exactly the same results in both cases; this unexpected behavior was revealed only when the values were compared to each other. From these results it is clear that the program is not effective in describing the lateral spreading in cases involving small scales. However, a better behavior was observed with regard to EC, where this counter-intuitive response was not found. To verify the effectiveness of CORMIX® in real case simulations, such an example has to be carried out and compared with the results obtained with Matlab model.

9   Conclusions

The results achieved with the mathematical simulation model are very satisfactory, considering the different behavior of the buoyant jet in the near and intermediate field. An average error of 0.28 and 0.37 was found, respectively, for the test with and without the presence of an inclined bottom. The model failed to give a proper description of the influence of the bottom slope through the parameter employed, and a new hypothesis is needed for modeling the entrainment process.

The commercial software CORMIX® did not properly reproduce the experimental results, giving inaccurate results for the bench scale simulations. The software is not able to provide the correct weight to the main parameters involved, yielding the same output for a whole set of experimental runs. However, this observation does not pertain to the general reliability of the program for natural scale applications.

Non-dimensional analysis showed how the dilution and lateral spreading of brine discharge in the near and intermediate field is not related to the initial hydraulic properties, as represented by the densimetric Froude and Reynolds numbers. It is anyway important to underline that is not under discussion the fact that in the near field, the jet properties are strongly dependent by the initial condition, but in the present study the presence of near and intermediate field is considered together, without trying to divide the two different zones.

The laboratory setup had some issues, mainly related with the subjectivity of the measurements and the difficulty to estimate the measurement accuracy.

10 References

Papers, articles

- Purnama A., Al-Barawi H. H. (2003). "Some criteria to minimize the impact of brine discharge into the sea" Desalination 17 (2004) 167-172.
- Douglas Baines W. (1985)."Entrainment by buoyant jet flowing along vertical walls" Journal of Hydraulic research 23 (1985) 221-228.

- Cipollina A., Brucato A., Grisafi F., Nicosia S. (2005) "Bench Scale Investigation of Inclined Dense Jets" Journal of Hydraulic engineering (ASCE) 131 (11), 1017–1022
- Al-Barwani H. H., Purnama A. (2007)."Simulating brine plumes discharged into the seawaters" Desalination 221 (2008) 608–613.
- Charcosset C. (2008)."A review of membrane processes and renewable energies for desalination." Desalination 245 (2009) 214–231.
- Christoudoulou G. C. (1991)."Dilution of dense effluents on a sloping bottom" Journal of Hydraulic research 29 (1991) 329-339.
- Cipollina A., Bonfiglio A., Micale G., Brucato B. (2004). "Dense jet modelling applied to the design of dense effluent diffusers." Desalination 167 (2004) 459-468.
- Cipollina A., Micale G., Rizzuti L." A critical assessment of desalination operations in Sicily." Desalination 182 (2005) 1–12
- Di Pinto A. C., Santori M. (1977) "Desalination activities in Italy" Desalination 20 (1977) 105-117
- Khawajia A. D.,. Kutubkhanaha I. K, Wieb J.M. (2007)."Advances in seawater desalination technologies" Desalination 221 (2008) 47–69.
- Lattemann S., Höpner T. (2007)." Environmental impact and impact assessment of seawater desalination." Desalination 220 (2008) 1–15.
- Rijsberman F. R (2005)."Water scarcity: Fact or fiction?" Agricultural Water Management 80 (2006) 5–22.
- Suresh P. R., Srinivasan K., Sundararajan T., Sarit Das K. (2008). " Reynolds number dependence of plane jet development in the transitional regime." Physics of fluids 20, (2008) 044105 1-12.

Books, seminaries, thesis

- Jönsson, L. (2004). "Receiving Water Hydraulics", Water Resources Engineering, Lund University.

- Fischer, J.L., Imberger, List, Koh, Brooks (1976)."Mixing in Inland and Coastal waters.", Academic Press.

- McCormick, Barnes W. (1979)."Aerodynamics, Aeronautics, and Flight Mechanics" John Wiley & Sons, Inc., New York.

- "IDA‟s Desalination Yearbook 2008-2009". Global Water Intelligence.

- Bashitialshaaer R. A. I., Flyborg L.,. Persson K. M (2009). "Environmental Assessment of Brine Discharge Including Wastewater Collection in the Arabian Gulf". IDA World Congress – Atlantis,The Palm – Dubai, UAE November 7-12.

- Sanchez D. (2009)." Near-field evolution and mixing of a negatively buoyant jet consisting of brine from a desalination plant". Thesis work at Water Resources Engineering, Department of Building and Environmental Technology, Lund University.

- Rognoni M (2009). "Dissalazione dellácqua del mare"

- Gerhard H. Jirka, Robert L. Doneker, And Steven W. Hinton (1996)."User's Manual For CORMIX[®]:A Hydrodynamic Mixing Zone Model And Decision Support System For Pollutant Discharges Into Surface Waters" DeFrees Hydraulics Laboratory School of Civil and Environmental Engineering, Cornell University

Web sites

- Water science for schools. Available at http://ga.water.usgs.gov/edu/earthwherewater.html
- United States Geological Survey. (updated 09 October 2009) Avaiable at: http://ga.water.usgs.gov/edu/waterdistribution.html

11   Appendix

Table 9 Laboratory measurements

RUN	S	ρ	Ø	Sb	Q	T tank	Ttracer	Y1	Y2	Y3	EC 1	EC2	EC3	Experimental t.	EC 1 after	EC2 after	EC3 after	Z1	Z2	Z3	Uo	Fr	Re
n	%	g/l	mm	cm/cm	l/min	°C	°C	cm	cm	cm	µS/cm	µS/cm	µS/cm	s	µS/cm	µS/cm	µS/cm	cm	cm	cm	m/s	ad.	ad.
25	4	1025,3	2,3	0,133	0,68	19,5	20,7	15,5	32,5	43,5				120	1480	1586	1670	10	15,5	17	2,73	111,3	5959,2
26	4	1025,3	2,3	0,133	0,4	19,5	20,7	18,0	37,5	50,0				120	450	880	970	8	10,5	11,5	1,61	65,5	3505,4
27	4	1025,3	2,3	0,133	0,7	21	20,7	4,0	15,5	29,0				80	1070	1090	1130	18	22	24	2,81	114,6	6134,5
28	4	1025,3	2,3	0,133	0,48	21	20,7	5,0	16,5	31,0				90	580	920	940	12	14,5	16	1,93	78,6	4206,5
29	4	1025,3	2,3	0,000	0,62	21,8	22	6,0	12,5	27,0	3900	2500	2300	100	1400	1650	1850	9	9	9	2,49	101,5	5433,4
30	4	1025,3	2,3	0,000	0,4	21,8	22	7,5	14,5	29,0	3400	2300	1600	100	1480	1520	1530	3	3	3	1,61	65,5	3505,4
31	4	1025,3	2,3	0,000	0,57	21,8	22	5,0	11,0	16,0	3800	1900	1300	80	1200	1450	1400	8	8	8	2,29	93,3	4995,2
32	4	1025,3	2,3	0,000	0,34	21,8	22	6,0	13,5	19,5	3900	1300	1200	100	1180	1250	1210	3	3	3	1,36	55,7	2979,6
33	4	1025,3	3,3	0,133	1,3	20,7	20,7	6,0	19,0	36,0				90	1900	2000	2100	14	18,5	21	2,53	86,3	7940,3
34	4	1025,3	3,3	0,133	0,7	20,7	20,7	9,0	20,0	45,0				90	1100	1300	1600	9,5	14	14,5	1,36	46,5	4275,5
35	4	1025,3	3,3	0,133	1,3	20,4	20,7	5,0	9,0	31,0				140	1400	1500	1600	27,5	32,5	35,5	2,53	86,3	7940,3
36	4	1025,3	3,3	0,133	0,7	20,4	20,7	6,0	16,0	43,0				150	1100	1100	1200	14	21	23,5	1,36	46,5	4275,5
37	4	1025,3	3,3	0,000	1,01	20,8	22	6,0	16,5	30,0	4000	2600	2300	70	1800	2200	2200	11	11	11	1,97	67,1	6169,0
38	4	1025,3	3,3	0,000	0,6	20,8	22	8,0	21,0	33,0	3900	2700	2300	90	900	1300	1600	4	4	4,5	1,17	39,8	3664,7
39	4	1025,3	3,3	0,000	1,04	20	22	4,0	14,0	26,0	4500	2300	1900	70	1400	1400	1400	12,5	12,5	12,5	2,03	69,1	6352,2
40	4	1025,3	3,3	0,000	0,61	20	22	5,5	15,5	31,0	3900	2200	1400	80	1300	1350	1400	5	5	5	1,19	40,5	3725,8
41	4	1025,3	4,8	0,133	1,14	21,5	21,5	33,0	45,0	53,0				120	2500	2700	2900	9	13	15,5	1,05	29,7	4787,1
42	4	1025,3	4,8	0,133	0,65	21,5	21,5	26,0	37,0	50,0				60	403	394	416	5	8,5	9,5	0,60	16,9	2729,5
43	4	1025,3	4,8	0,133	1,13	20,5	21,5	39,0	46,0	53,0				100	1480	1550	1720	9	13,5	17	1,04	29,4	4745,1
44	4	1025,3	4,8	0,133	0,68	20,5	21,5	35,0	43,0	51,0				75	480	670	967	3	6	9	0,63	17,7	2855,4
45	4	1025,3	4,8	0,000	1,24	19,8	22	10,0	24,0	35,5	5100	2900	2300	110	1600	2600	2900	12	12	11,5	1,14	32,3	5207,0
46	4	1025,3	4,8	0,000	0,79	19,8	22	13,0	27,0	37,0	3800	2600	2300	90	1500	1800	3100	5	5	5	0,73	20,6	3317,4
47	4	1025,3	4,8	0,000	1,3	21	22	7,5	20,0	30,0	5200	5100	2400	100	2100	2200	2300	18	18	17,5	1,20	33,8	5458,9
48	4	1025,3	4,8	0,000	0,72	21	22	10,5	25,0	36,0	4600	2100	1600	90	1900	2300	2300	5	5	5	0,66	18,7	3023,4
49	6	1038,5	2,3	0,133	0,77	20,7	20,7	16,0	25,5	38,0	4500	3200	2800	130	2200	2400	2600	9	14	18	3,09	104,2	6834,5
50	6	1038,5	2,3	0,133	0,53	20,7	20,7	22,0	32,0	42,0	3120	2000	1450	120	1200	1500	1750	6	9	12,5	2,13	71,7	4704,3
51	6	1038,5	2,3	0,133	0,77	20,5	20,7	11,0	20,0	32,5				90	1330	1400	1440	17,5	22	25	3,09	104,2	6834,5
52	6	1038,5	2,3	0,133	0,55	20,5	20,7	17,0	30,5	44,0				100	940	1060	1110	12	15	18	2,21	74,5	4881,8
53	6	1038,5	2,3	0,000	0,63	20	20,2	9,5	21,0	28,5	4500	3100	2600	70	1700	2500	2600	9	9	9	2,53	85,3	5591,8
54	6	1038,5	2,3	0,000	0,37	20	20,2	13,0	26,5	35,5	4100	2600	2400	90	600	1600	2000	5	4,5	4,5	1,48	50,1	3284,1
55	6	1038,5	2,3	0,000	0,6	20,8	20,2	5,0	11,0	14,0	3800	2500	1300	80	1500	1500	1500	8	8	8	2,41	81,2	5325,6
56	6	1038,5	2,3	0,000	0,41	20,8	20,2	7,0	13,0	16,0	3100	2200	1300	100	1400	1300	1400	3	3	3	1,65	55,5	3639,1
57	6	1038,5	3,3	0,133	1,19	19,5	20,7	25,0	38,0	46,0				70	2200	2300	2330	8,5	12	16	2,32	65,3	7361,7
58	6	1038,5	3,3	0,133	0,8	19,5	20,7	23,0	42,0	48,0				60	470	720	1600	5	7,5	10,5	1,56	43,9	4949,0
59	6	1038,5	3,3	0,133	1,07	19,4	20,7	21,0	33,0	42,0				80	1500	1650	1670	16	22	26,5	2,09	58,7	6619,3
60	6	1038,5	3,3	0,133	0,78	19,4	20,7	25,0	37,0	46,0				110	1260	1310	1320	10	12,5	14	1,52	42,8	4825,3
61	6	1038,5	3,3	0,000	0,93	22	20,2	13,0	22,0	32,5	6300	3300	3100	120	3000	3300	3500	10,5	10,5	10,5	1,81	51,1	5753,2
62	6	1038,5	3,3	0,000	0,63	22	20,2	15,0	25,5	37,5	5300	3600	1300	90	1100	2300	3100	6,5	6,5	6	1,23	34,6	3897,3
63	6	1038,5	3,3	0,000	1,04	19,8	20,2	5,5	16,0	22,0	5500	3300	1100	90	1900	2000	1900	14	14	14	2,03	57,1	6433,7
64	6	1038,5	3,3	0,000	0,58	19,8	20,2	7,0	19,0	25,5	4900	2000	1800	100	1800	1900	2200	5	5	5	1,13	31,8	3588,0
65	6	1038,5	4,8	0,133	1,43	19,4	20,7	40,0	48,0	53,0				90	2800	3200	3400	10	13	16,5	1,32	30,8	6081,9
66	6	1038,5	4,8	0,133	0,85	19,4	20,7	36,0	43,0	50,0				60	550	660	1300	4	5,5	7,5	0,78	18,3	3615,1
67	6	1038,5	4,8	0,133	1,17	19,8	20,7	31,5	43,0	53,0				150	2300	2500	2600	13,5	17,5	20,5	1,08	25,2	4976,1
68	6	1038,5	4,8	0,133	0,87	19,8	20,7	33,0	41,0	53,0				75	1205	1500	1700	7,5	9,5	12	0,80	18,7	3700,2
69	6	1038,5	4,8	0,000	1,27	20,6	20,2	13,0	26,0	33,5	7500	5000	3500	80	3300	3900	4300	9	9	9	1,17	27,3	5401,4
70	6	1038,5	4,8	0,000	0,89	20,6	20,2	21,0	30,0	40,0	4000	3600	2700	90	2400	3400	3600	4	4	4,5	0,82	19,1	3785,2
71	6	1038,5	4,8	0,000	1,01	20,2	20,2	15,0	23,0	32,0	6300	3000	2900	100	3200	3400	3400	12	12	12	0,93	21,7	4295,6
72	6	1038,5	4,8	0,000	0,87	20,2	20,2	17,0	26,0	35,0	5800	3100	2500	120	900	2800	3100	7,5	7,5	7,5	0,80	18,7	3700,2
1	8	1050,9	2,3	0,133	0,64	22	21,5	21,5	30,5	34,5	6500	4300	3900	90	2700	3100	3400	8	12	15	2,57	76,2	5748,7
2	8	1050,9	2,3	0,133	0,43	22	21,5	22,5	34,5	40,0	3400	2400	2000	150	1300	1900	2400	4,5	8	12	1,73	51,2	3862,4
3	8	1050,9	2,3	0,133	0,7	20,9	21,5	8,5	20,0	30,0	6000	3600	2300	80	1840	1900	2030	15	18,5	23	2,81	83,4	6287,7
4	8	1050,9	2,3	0,133	0,48	20,9	21,5	12,0	25,5	36,5	4900	1500	1000	130	860	1300	1400	6	8	10,5	1,93	57,2	4311,5
5	8	1050,9	2,3	0,000	0,67	20,1	21,2	11,0	19,5	30,0	6200	4300	2700	80	2100	3200	3500	10	10,5	10,5	2,69	79,8	6018,2
6	8	1050,9	2,3	0,000	0,42	20,1	21,2	14,5	23,5	32,0	5200	3000	2300	90	500	1200	2800	5	5	5	1,69	50,0	3772,6
7	8	1050,9	2,3	0,000	0,61	20	21,2	8,0	14,0	20,0	5200	2600	1800	90	2100	2200	2200	15	15	15	2,45	72,6	5479,2
8	8	1050,9	2,3	0,000	0,43	20	21,2	11,0	19,0	27,0	4400	1900	1300	150	1750	1810	2010	6,5	6,5	6,5	1,73	51,2	3862,4
9	8	1050,9	3,3	0,133	1,05	20,9	21,5	19,5	30,0	38,0	7500	5100	4500	150	3500	4300	4400	10,5	14,5	17	2,05	50,7	6573,5
10	8	1050,9	3,3	0,133	0,63	20,9	21,5	24,0	36,0	43,0	4500	3400	2400	160	1300	2100	2800	7,5	10	13,5	1,23	30,4	3944,1
11	8	1050,9	3,3	0,133	1,15	19,7	21,5	11,0	21,0	28,0	4900	3000	2400	90	1900	2100	2300	17,5	21	24	2,24	55,5	7199,5
12	8	1050,9	3,3	0,133	0,67	19,7	21,5	21,0	36,0	42,0	3800	1400	1200	110	1300	1500	1600	9,5	12,5	15,5	1,31	32,4	4194,5
13	8	1050,9	3,3	0,000	1,05	20,9	21,2	20,0	32,5	40,0	9300	5400	3900	80	3100	3300	3500	12	12	12	2,05	50,7	6573,5
14	8	1050,9	3,3	0,000	0,7	20,9	21,2	28,5	40,0	47,0	6600	3200	2600	70	2300	3400	3700	6	6	6	1,36	33,8	4382,3
15	8	1050,9	3,3	0,000	1,06	20,3	21,2	9,0	23,5	36,0	7400	2900	1900	60	2500	2700	2700	14,5	15,5	16	2,07	51,2	6636,1
16	8	1050,9	3,3	0,000	0,71	20,3	21,2	16,5	30,0	42,0	5000	3400	2100	110	1400	2200	2300	9	10	10	1,38	34,3	4444,9
17	8	1050,9	4,8	0,133	1,21	20,9	21,5	28,0	37,5	39,0	7500	5200	4800	100	3500	4600	4800	8,5	11,5	16	1,12	22,9	5207,9
18	8	1050,9	4,8	0,133	0,91	20,9	21,5	32,0	40,0	48,0	4900	3500	3100	120	1100	2400	2700	6	8	13	0,84	17,2	3916,7
19	8	1050,9	4,8	0,133	1,43	22,5	21,5	25,0	35,0	44,0	6900	3100	2700	90	2700	3200	3400	17	21,5	25,5	1,32	27,1	6154,8
20	8	1050,9	4,8	0,133	0,97	22,5	21,5	29,0	39,0	50,0	5300	2000	1900	130	1700	2000	2200	10	13	17,5	0,89	18,4	4174,9
21	8	1050,9	4,8	0,000	1,17	20,2	21,2	27,0	36,5	35,0	7900	5500	6100	90	5600	6400	6600	7,5	7,5	7,5	1,08	22,1	5035,7
22	8	1050,9	4,8	0,000	0,9	20,2	21,2	36,5	43,5	48,0	6000	4300	5300	270	3400	3900	4400	6,5	6,5	6,5	0,83	17,0	3873,6
23	8	1050,9	4,8	0,000	1,25	21	21,2	23,0	32,5	39,5	8500	5800	4800	110	4500	5100	4800	13	13,5	13,5	1,15	23,7	5380,1
24	8	1050,9	4,8	0,000	0,89	21	21,2	27,0	39,0	46,5	4800	2400	2300	280	2600	3400	3600	8	8	7	0,82	16,8	3830,6

Table 10 R^2 coefficient for y/D and Froude numbers correlations

y1

Θ = 0	y1			Θ = 0	y1				Sb = 0	y1				Θ = 0	y1		
S/Sb	0	15	Average	S/φ	0.0023	0.0033	0.0048	Average	S/φ	0.0023	0.0033	0.0048	Average	φ/Sb	0	15	Average
4	0,012	0,003	0,007	4	0,007	0,721	0,015	0,248	4	0,261	0,417	0,571	0,417	0,0023	0,636	0,691	0,663
6	0,036	0,002	0,019	6	0,000	0,288	0,007	0,098	6	0,243	0,080	0,650	0,324	0,0033	0,322	0,300	0,311
8	0,372	0,439	0,405	8	0,082	0,695	0,805	0,527	8	0,385	0,353	0,496	0,411	0,0048	0,545	0,299	0,422
Average	0,140	0,148	0,144	Average	0,030	0,568	0,276	0,291	Average	0,296	0,283	0,572	0,384	Average	0,501	0,430	0,466
Θ = 30	y1			Θ = 30	y1				Sb = 15	y1				Θ = 30	y1		
S/Sb	0	15	Average	S/φ	0.0023	0.0033	0.0048	Average	S/φ	0.0023	0.0033	0.0048	Average	φ/Sb	0	15	Average
4	0,000	0,642	0,321	4	0,941	0,364	0,038	0,448	4	0,114	0,444	0,368	0,309	0,0023	0,437	0,252	0,344
6	0,354	0,354	0,354	6	0,027	0,021	0,053	0,034	6	0,631	0,011	0,275	0,306	0,0033	0,323	0,356	0,340
8	0,552	0,588	0,570	8	0,716	0,840	0,508	0,688	8	0,181	0,723	0,883	0,596	0,0048	0,335	0,006	0,170
Average	0,302	0,528	0,415	Average	0,561	0,408	0,200	0,390	Average	0,309	0,393	0,509	0,403	Average	0,365	0,205	0,285

y2

Θ = 0	y2			Θ = 0	y2				Sb = 0	y2				Θ = 0	y2		
S/Sb	0	15	Average	S/φ	0.0023	0.0033	0.0048	Average	S/φ	0.0023	0.0033	0.0048	Average	φ/Sb	0	15	Average
4	0,005	0,154	0,080	4	0,002	0,343	0,005	0,117	4	0,536	0,364	0,635	0,512	0,0023	0,524	0,379	0,452
6	0,318	0,239	0,279	6	0,106	0,103	0,038	0,082	6	0,115	0,261	0,092	0,156	0,0033	0,352	0,233	0,293
8	0,000	0,497	0,248	8	0,145	0,708	0,762	0,538	8	0,311	0,379	0,785	0,492	0,0048	0,517	0,577	0,547
Average	0,108	0,297	0,202	Average	0,085	0,384	0,268	0,246	Average	0,321	0,335	0,504	0,387	Average	0,464	0,397	0,430
Θ = 30	y2			Θ = 30	y2				Sb = 15 %	y2/D				Θ = 30	y2		
S/Sb	0	15	Average	S/φ	0.0023	0.0033	0.0048	Average	*S/φ*	*0.0023*	*0.0033*	*0.0048*	*Average*	φ/Sb	0	15	Average
4	0,007	0,280	0,144	4	0,010	0,853	0,068	0,310	4	0,126	0,216	0,660	0,334	0,0023	0,527	0,404	0,466
6	0,108	0,055	0,081	6	0,033	0,011	0,116	0,053	6	0,826	0,202	0,773	0,601	0,0033	0,300	0,532	0,416
8	0,224	0,005	0,115	8	0,126	0,910	0,646	0,561	8	0,419	0,853	0,981	0,751	0,0048	0,342	0,013	0,177
Average	0,113	0,113	0,113	Average	0,056	0,591	0,276	0,308	**Average**	0,457	0,424	0,805	0,562	Average	0,390	0,316	0,353

y3

Θ = 0	y3			Θ = 0	y3				Sb = 0	y3				Θ = 0	y3		
S/Sb	0	15	Average	S/φ	0.0023	0.0033	0.0048	Average	S/φ	0.0023	0.0033	0.0048	Average	φ/Sb	0	15	Average
4	0,567	0,299	0,433	4	0,013	0,064	0,037	0,038	4	0,001	0,666	0,531	0,399	0,0023	0,733	0,017	0,375
6	0,337	0,680	0,509	6	0,004	0,078	0,005	0,029	6	0,086	0,163	0,267	0,172	0,0033	0,427	0,276	0,352
8	0,347	0,492	0,420	8	0,264	0,679	0,881	0,608	8	0,121	0,700	0,770	0,530	0,0048	0,486	0,107	0,297
Average	0,417	0,491	0,454	Average	0,094	0,274	0,308	0,225	Average	0,069	0,509	0,523	0,367	Average	0,549	0,133	0,341
Θ = 30	y3			Θ = 30	y3				Sb = 15 %	y3/D				Θ = 30	y3		
S/Sb	0	15	Average	S/φ	0.0023	0.0033	0.0048	Average	*S/φ*	*0.0023*	*0.0033*	*0.0048*	*Average*	φ/Sb	0	15	Average
4	0,006	0,056	0,031	4	0,098	0,214	0,101	0,137	**4**	0,193	0,884	0,948	0,675	0,0023	0,374	0,308	0,341
6	0,470	0,378	0,424	6	0,114	0,013	0,077	0,068	**6**	0,758	0,247	0,310	0,438	0,0033	0,190	0,412	0,301
8	0,001	0,162	0,082	8	0,069	0,870	0,410	0,450	**8**	0,889	0,784	0,416	0,696	0,0048	0,404	0,031	0,218
Average	0,159	0,199	0,179	Average	0,094	0,366	0,196	0,218	**Average**	0,613	0,638	0,558	0,603	Average	0,323	0,250	0,287

Table 11 R^2 coefficient for m, b and Froude numbers correlations

m

Θ = 0	m			Θ = 0	m				Sb = 0	m				Θ = 0	m		
S/Sb	0	15	Average	S/φ	0.0023	0.0033	0.0048	Average	S/φ	0.0023	0.0033	0.0048	Average	φ/Sb	0	15	Average
4	0,927	0,295	0,611	4	0,010	0,061	0,031	0,034	4	0,003	0,646	0,538	0,396	0,0023	0,651	0,009	0,330
6	0,711	0,795	0,753	6	0,025	0,054	0,013	0,031	6	0,079	0,203	0,113	0,132	0,0033	0,434	0,222	0,328
8	0,425	0,641	0,533	8	0,279	0,675	0,869	0,608	8	0,123	0,746	0,779	0,549	0,0048	0,411	0,123	0,267
Average	0,688	0,577	0,632	Average	0,105	0,263	0,304	0,224	Average	0,068	0,532	0,477	0,359	Average	0,499	0,118	0,308
Θ = 30	m			Θ = 30	m				Sb = 15	m				Θ = 30	m		
S/Sb	*0*	*15*	**Average**	S/φ	0.0023	0.0033	0.0048	Average	S/φ	0.0023	0.0033	0.0048	Average	φ/Sb	0	15	Average
4	0,807	0,892	*0,850*	4	0,102	0,310	0,129	0,180	4	0,188	0,783	0,816	0,596	0,0023	0,387	0,347	0,367
6	0,883	0,894	*0,889*	6	0,108	0,010	0,096	0,071	6	0,749	0,261	0,285	0,432	0,0033	0,195	0,511	0,353
8	0,811	0,761	*0,786*	8	0,052	0,839	0,450	0,447	8	0,960	0,815	0,372	0,716	0,0048	0,367	0,032	0,199
Average	*0,834*	*0,849*	*0,841*	Average	0,087	0,386	0,225	0,233	Average	0,633	0,620	0,491	0,581	Average	0,317	0,296	0,306

b

Θ = 0	b			Θ = 0	b				Sb = 0	b				Θ = 0	b		
S/Sb	0	15	Average	S/φ	0.0023	0.0033	0.0048	Average	S/φ	0.0023	0.0033	0.0048	Average	φ/Sb	0	15	Average
4	0,863	0,166	0,515	4	0,000	0,092	0,005	0,032	4	0,116	0,061	0,489	0,222	0,0023	0,463	0,394	0,428
6	0,539	0,647	0,593	6	0,003	0,387	0,014	0,134	6	0,869	0,035	0,750	0,552	0,0033	0,283	0,220	0,251
8	0,903	0,220	0,562	8	0,043	0,706	0,300	0,350	8	0,708	0,261	0,188	0,385	0,0048	0,478	0,297	0,388
Average	0,769	0,345	0,557	Average	0,015	0,395	0,106	0,172	Average	0,564	0,119	0,476	0,386	Average	0,408	0,303	0,356
Θ = 30°	b			Θ = 30	b				Sb = 15	b				Θ = 30	b		
S/Sb	*0*	*15*	**Average**	S/φ	0.0023	0.0033	0.0048	Average	S/φ	0.0023	0.0033	0.0048	Average	φ/Sb	0	15	Average
4	0,005	0,580	*0,293*	4	0,270	0,027	0,025	0,107	4	0,056	0,527	0,338	0,307	0,0023	0,269	0,221	0,245
6	0,128	0,918	*0,523*	6	0,776	0,026	0,054	0,285	6	0,449	0,000	0,232	0,227	0,0033	0,278	0,258	0,268
8	0,490	0,930	*0,710*	8	0,468	0,487	0,800	0,585	8	0,079	0,729	0,280	0,363	0,0048	0,276	0,031	0,154
Average	*0,208*	*0,809*	*0,509*	Average	0,505	0,180	0,293	0,326	Average	0,194	0,419	0,284	0,299	Average	0,274	0,170	0,222

Table 12 Effects of geometrical parameters on lateral spreading

| S	φ	Δ Y1 /D				Δ Y2 /D				Δ Y3 /D			
%	mm	Θ = 0, Sb = 0	Θ = 0, Sb = 15	Θ = 30, Sb = 15	Θ = 30, Sb = 0	Θ = 0, Sb = 0	Θ = 0, Sb = 15	Θ = 30, Sb = 15	Θ = 30, Sb = 0	Θ = 0, Sb = 0	Θ = 0, Sb = 15	Θ = 30, Sb = 15	Θ = 30, Sb = 0
4	2,3	0,0	41,3	-8,7	-4,3	0,0	87,0	13,0	-6,5	0,0	71,7	8,7	-47,8
4	2,3	0,0	45,7	-10,9	-6,5	0,0	100,0	8,7	-4,3	0,0	91,3	8,7	-41,3
4	3,3	0,0	0,0	-3,0	-6,1	0,0	7,6	-22,7	-7,6	0,0	18,2	3,0	-12,1
4	3,3	0,0	3,0	-6,1	-7,6	0,0	-3,0	-15,2	-16,7	0,0	36,4	30,3	-6,1
4	4,8	0,0	47,9	60,4	-5,2	0,0	43,8	45,8	-8,3	0,0	36,5	36,5	-11,5
4	4,8	0,0	27,1	45,8	-5,2	0,0	20,8	33,3	-4,2	0,0	27,1	29,2	-2,1
6	2,3	0,0	28,3	6,5	-19,6	0,0	19,6	-4,3	-43,5	0,0	41,3	17,4	-63,0
6	2,3	0,0	39,1	17,4	-26,1	0,0	23,9	17,4	-58,7	0,0	28,3	37,0	-84,8
6	3,3	0,0	36,4	24,2	-22,7	0,0	48,5	33,3	-18,2	0,0	40,9	28,8	-31,8
6	3,3	0,0	24,2	30,3	-24,2	0,0	50,0	34,8	-19,7	0,0	31,8	25,8	-36,4
6	4,8	0,0	56,3	38,5	4,2	0,0	45,8	35,4	-6,3	0,0	40,6	40,6	-3,1
6	4,8	0,0	31,3	25,0	-8,3	0,0	27,1	22,9	-8,3	0,0	20,8	27,1	-10,4
8	2,3	0,0	45,7	-10,9	-13,0	0,0	47,8	2,2	-23,9	0,0	19,6	0,0	-43,5
8	2,3	0,0	34,8	-10,9	-15,2	0,0	47,8	8,7	-19,6	0,0	34,8	19,6	-21,7
8	3,3	0,0	-1,5	-27,3	-33,3	0,0	-7,6	-34,8	-27,3	0,0	-6,1	-36,4	-12,1
8	3,3	0,0	-13,6	-22,7	-36,4	0,0	-12,1	-12,1	-30,3	0,0	-12,1	-15,2	-15,2
8	4,8	0,0	2,1	-4,2	-8,3	0,0	2,1	-3,1	-8,3	0,0	8,3	18,8	9,4
8	4,8	0,0	-9,4	-15,6	-19,8	0,0	-7,3	-9,4	-9,4	0,0	0,0	4,2	-3,1
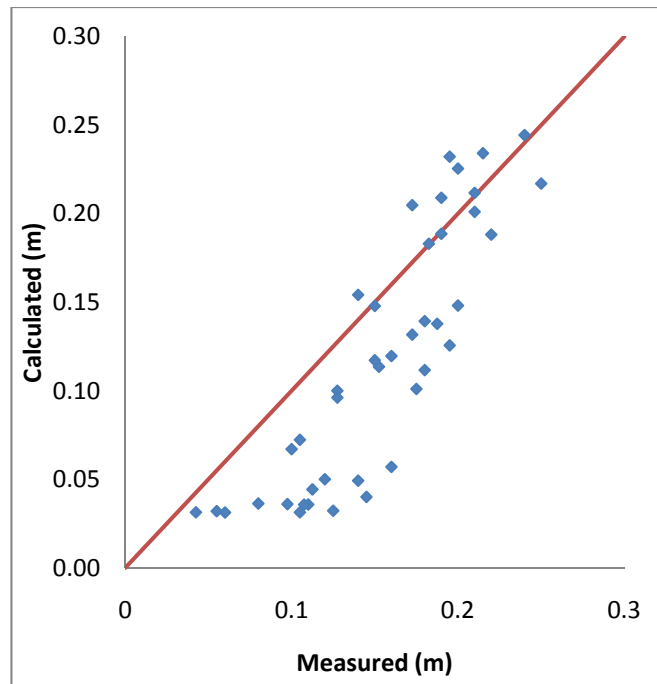
Figure 31 Calculated versus measured half spreading (b), bottom slope = 7.66°
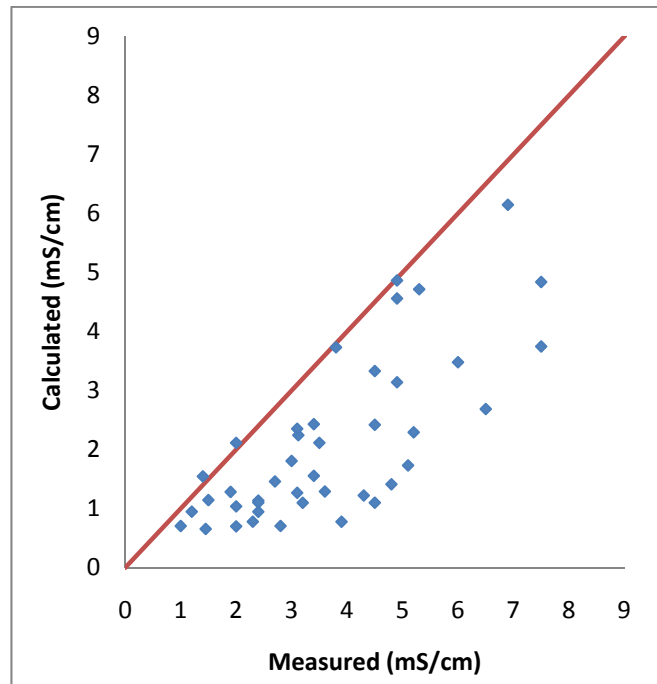
Figure 32 Calculated versus measured electrical conductivity, bottom slope = 7.66°

The CORMIX® Prediction File is a detailed listing of all simulation input data as well as the predicted plume properties (plume shapes and concentration distributions) arranged by the individual flow modules that form part of the simulation.

In table 13 is shown as example one of the output file of CORMIX® for run 54, displaying the beginning of the simulation in the near-field mixing region.

Run 20

Φ= 4.8 mm

Θ= 30 °

Sb= 7.66°

S= 8 %

Run 21

Φ= 4.8 mm

Θ= 0 °

Sb= 0°

S= 8 %

The software reports that already in the near-field region it has detected a bottom-attached jet. This behavior is expected being a case with the jet pointing parallel to the bottom (Θ= 0°).

The first three columns gives the x, y, z position of the jet or plume centerline, S and C columns give, respectively, the dilution and the concentration along the centerline, and the most interesting for our study, B that represents the jet width or as in our case the spreading. The jet half-width is given as 1/e of a Gaussian curve, equivalent to 37% of the peak value. To be able to plot the measured versus calculated values it is necessary to multiply by 2 (half width) and divide by 0.37 (figure 33).
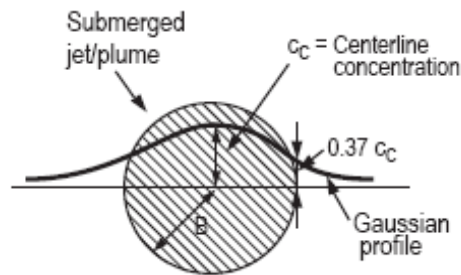

Figure 33 Submerged jet/plume Gaussian profile used to calculate the concentration

Table 13 Example of a CORMIX® prediction file imported into Excel

x	y	z	S	C	b
0	0	-0,3	1	8,00E+00	0
0	-0,03	-0,3	1,6	4,92E+00	0,01
0	-0,07	-0,3	2,5	3,14E+00	0,01
0	-0,11	-0,3	3,6	2,23E+00	0,01
0	-0,14	-0,3	4,5	1,78E+00	0,02
0	-0,18	-0,3	5,5	1,44E+00	0,02
0	-0,21	-0,3	6,5	1,24E+00	0,03
0	-0,25	-0,3	7,5	1,07E+00	0,03
0	-0,29	-0,3	8,4	9,51E-01	0,03
0	-0,32	-0,3	9,5	8,47E-01	0,04
0	-0,36	-0,3	10,4	7,71E-01	0,04
0	-0,4	-0,3	11,4	7,01E-01	0,05
0	-0,43	-0,3	12,3	6,49E-01	0,05
0	-0,47	-0,3	13,4	5,99E-01	0,05
0	-0,5	-0,3	14,3	5,60E-01	0,06
0	-0,54	-0,3	15,2	5,26E-01	0,06
0	-0,57	-0,3	16,2	4,93E-01	0,07
0	-0,61	-0,3	17,2	4,66E-01	0,07

Table 14 Comparison between CORMIX® and measured values for conductivity

x	Cormix		Conductivity for salinity at 6%			x	Measured	Corrected	
0	100,00		81000	mS/cm		0	100,00	100,00	
0,03	37,50					0,2	4,10	5,06	
0,07	21,17					0,4	2,60	3,21	
0,11	14,70		Mean Square error			0,6	2,40	2,96	
0,14	11,27								
0,18	9,23			2,12					
0,22	7,75								
0,25	6,68		Root Mean Square error						
0,29	5,87								
0,32	5,27			1,46					
0,36	4,75								
0,4	4,32								
0,43	3,97								
0,47	3,68								
0,51	3,42								
0,54	3,20								
0,58	3,00								
0,61	2,83								

The first thing is to express the concentration values C in terms of percentage, considering the origin concentration (ex. 6 g/l) to be equal to 100 %, and dividing the following points by the original concentration (table 14). For the experimental points three measurements are available, at 20, 40 and 60 cm. The probe used during the experiments showed some problems in reading the conductivity at very high concentrations, so all values have been normalized with the correct standard salinity. To obtain this, a different probe was used, more precise, but it was not sufficiently responsive to be used during the tests. Even if the correction is not so relevant it is formally correct.

On the left are reported the concentration values obtained with CORMIX$^{®}$ at the corresponding x point and on the right of the chart the measured values. In case the concentration value obtained with the software is estimated for a different point with respect to the point used for the measurement, the closest one is chosen.

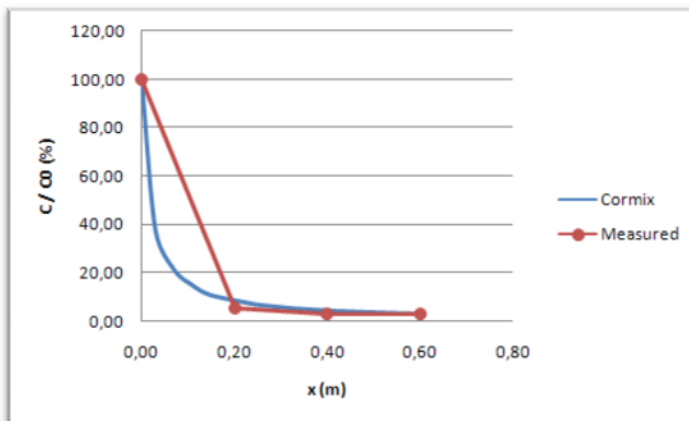The results are plotted in figure 34, showing a case without bottom slope and a vertical angle of 0.

Figure 34 Comparison between Measured values and CORMIX evaluation for Concentration

The Mean Square error is around 2 % and the Root Mean Square error around 1.5%.

Table 15 Comparison between CORMIX® and Measured spreading

x	Cormix spreading		x	Measured spreading
0,00	0,00		0	0
0,03	0,05		0,2	0
0,07	0,05		0,4	0
0,11	0,05		0,6	0
0,14	0,11			
0,18	0,11		Mean Square error	
0,22	0,16			
0,25	0,16			0,14
0,29	0,16			
0,32	0,22		Root Mean Square error	
0,36	0,22			
0,40	0,27			0,37
0,43	0,27			
0,47	0,27			
0,51	0,32			
0,54	0,32			
0,58	0,38			
0,61	0,38			

The same procedure is followed for the spreading shown in table 15; on the left are the CORMIX® values and on the right the measurements. For every run is also calculated the average Mean Square error and Root Mean Square error, both for concentration and spreading.

As stated before, for run 20 and 21, even if the main parameters are different, the same results are obtained for the spreading in CORMIX®. This result implies that the model is not reliable for our purposes, but better agreement is expected for application at field scale.